
# Bi-level ramp merging coordination for dense mixed traffic conditions

Fundamental Research xxx (xxxx) xxx

Contents lists available at ScienceDirect

Fundamental Research

journal homepage: http://www.keaipublishing.com/en/journals/fundamental-research/

Article

# Bi-level ramp merging coordination for dense mixed traffic conditions

Jie Zhu[a], Kun Gao[a,*], Hao Li[b], Zijing He[c], Cristina Olaverri Monreal[d]

[a] Department of Architecture and Civil Engineering, Chalmers University of Technology, Gothenburg 41296, Sweden
[b] College of Transportation Engineering, Tongji University, Shanghai 201804, China
[c] Department of Psychology, Sun Yat-sen University, Guangzhou 510275, China
[d] The Chair for Sustainable Transport Logistics 4.0, Johannes Kepler University Linz, 4040, Austria

ARTICLE INFO

*Article history:*
Received 6 September 2022
Received in revised form 8 February 2023
Accepted 23 March 2023
Available online xxx

*Keywords:*
Ramp merging coordination
Connected and autonomous vehicles
Freeway on-ramps
Mixed traffic
Bi-level strategy

ABSTRACT

Connected and Autonomous Vehicles (CAVs) hold great potential to improve traffic efficiency, emissions and safety in freeway on-ramp bottlenecks through coordination between mainstream and on-ramp vehicles. This study proposes a bi-level coordination strategy for freeway on-ramp merging of mixed traffic consisting of CAVs and human-driven vehicles (HDVs) to optimize the overall traffic efficiency and safety in congested traffic scenarios at the traffic flow level instead of platoon levels. The macro level employs an optimization model based on fundamental diagrams and shock wave theories to make optimal coordination decisions, including optimal minimum merging platoon size to trigger merging coordination and optimal coordination speed, based on macroscopic traffic state in mainline and ramp (i.e., traffic volume and penetration rates of CAVs). Furthermore, the micro level determines the real platoon size in each merging cycle as per random arrival patterns and designs the coordinated trajectories of the mainline facilitating vehicle and ramp platoon. A receding horizon scheme is implemented to accommodate human drivers' stochastics as well. The developed bi-level strategy is tested in terms of improving efficiency and safety in a simulation-based case study under various traffic volumes and CAV penetration rates. The results show the proposed coordination addresses the uncertainties in mixed traffic as expected and substantially improves ramp merging operation in terms of merging efficiency and traffic robustness, and reducing collision risk and emissions, especially under high traffic volume conditions.

## 1. Introduction

Freeway on-ramps are typical bottlenecks in the freeway network, as merging maneuvers of on-ramp vehicles impose frequent disturbances on the mainline traffic flow and lead to reduced traffic efficiency and increased collision risk. Traditional traffic management measures, such as ramp metering [1,2] and variable speed limits [3,4], are shown to improve the merging operation at freeway on-ramps, but the improvements are limited as those measures can only manage traffic at an aggregated level without manipulating the microscopic interactions between individual vehicles.

The emerging Connected and Autonomous Vehicles (CAVs) bring substantial improvements in traffic operation in ramp merging. With advanced communication and autonomous driving technologies, the motions of individual vehicles can be planned in advance and executed in a precise and timely manner, enabling opportunities for cooperative driving in the on-ramp merging areas [5,6]. Most notably, Wang et al. [7] made a critical contribution to the long-unsettled problem of automated driving assistance. This seminal work substantially improved the adaptability of driving assistance to different drivers, thus increasing the acceptance of the longitudinal Advanced Driving Assistance System (ADAS) by drivers. Other cooperative strategies have also been proposed to facilitate the ramp merging operation of CAVs. We refer to our previous work for a thorough review of this topic [8]. In summary, a major focus in this research field is to coordinate the motion plans or trajectories of multiple vehicles by means of optimization, game theory, learning-based approaches, etc. The early research efforts mainly focused on the interaction between a ramp merging vehicle and its direct neighbors in the merging process [7,9–12], while later the coordination scope was extended to a collection of vehicles in a pre-assumed communication range [13–17]. In some recent studies, the research focus has been shifted to the upper-level considerations, and some previously untouched topics such as the optimal merging gap and merging sequence, are more frequently discussed [18–21]. However, all the studies have assumed a full CAV context where all vehicles are readily controllable and cannot be directly applied to situations where Human-Driven Vehicles (HDVs) exist.

It is widely agreed that the full launch of CAVs will not happen immediately, and there will be a long period when the CAVs and HDVs interact with each other on public roads. Merging coordination in such mixed

* Corresponding author.
*E-mail address:* gkun@chalmers.se (K. Gao).

https://doi.org/10.1016/j.fmre.2023.03.015

traffic conditions is more challenging because the presence of uncontrollable HDVs will introduce more uncertainties into real-time traffic operations. Recent research has been targeting such mixed traffic challenges. A major effort is to predict the driving intentions of human drivers and use the predictions of HDVs as inputs for CAV motion planning [22–25]. The prediction errors are continuously measured and tackled using the model predictive control mechanism [26]. In a pioneering study, Qu et al. [27] has made a breakthrough in modeling four distinct scenarios (HDV only, AV only, mixed traffic with CAV and HDV, and cooperative CAVs) in a context of transportation infrastructure with multiple control units, in terms of the safety, efficiency and sustainability. According to their results, AVs alone could increase energy consumption and travel time, while cooperative CAVs will have collective benefits. Though taking human decisions into account, the approaches only regard HDVs as an uncontrolled external factor that restricts CAV behaviors while not fully exploiting the possibilities of influencing HDV behaviors through surrounding CAVs for enhanced coordination benefits.

Furthermore, these studies mainly focus on the lower-level trajectory decisions of individual vehicles (namely, merely optimizing the trajectories of several vehicles) rather than the overall optimum at the traffic flow level. This may lead to sub-optimal solutions at the continuous traffic flow level, as the deceleration of mainline vehicles (i.e., creating gaps of ramp vehicles) would cause shock waves and affect the speeds of the following vehicles. Particularly, the dilemma is very considerable when traffic volumes in the mainline and ramp are very high, and merging takes place frequently. When the traffic flow volumes in the mainline and ramps are very large, and the merging frequency of ramp platoons is high, local coordination merely considering a vehicle platoon on the ramp and several vehicles in the mainline may result in undispersed shockwaves in the mainline and impair the overall traffic efficiency in mainline. In this regard, the merging coordination should not only focus on the coordination of serval vehicles but also take the overall traffic efficiency at the continuous traffic flow level. Hence, further efforts on coordination for mixed traffic with HDVs and CAVs to optimize the overall efficiency and safety at the continuous traffic flow level are needed to facilitate the development of CAVs for the forthcoming mixed traffic environment.

Standing in the wake of existing research, this study develops a novel coordination strategy to optimize ramp merging operation in mixed traffic with a focus on overall efficiency and safety at the traffic flow level instead of the platoon level. Specific emphasis is put on the scenario where traffic volumes in the mainline and ramp are very large, and the frequent merging of ramp platoons will impose significant disturbance in the mainline traffic. This strategy leverages CAVs as actuators to regulate the motions of surrounding HDVs. The proposed coordination strategy consists of two levels. The macro level is formulated as an optimization problem utilizing traffic fundamental diagrams and shock wave theories to determine the optimal coordination plan according to the macroscopic traffic state in the merging area, including penetration rates of CAVs, traffic volumes in the mainline and ramp. The micro level designs the trajectories of mainline facilitating vehicles and ramp platoon to accommodate uncertainties and stochastic patterns in real-time traffic operation based on a receding horizon scheme. The benefits of the proposed bi-level coordination strategy are validated through SUMO-based simulation case studies considering heterogeneity in human drivers and under different traffic volumes and CAV penetration rates.

The following parts of the paper are structured as follows. Section 2 presents an overview of the proposed coordination strategy, followed by detailed formulations of the bi-level model in Section 3. Section 4 introduces the setup of the SUMO-based simulation and case studies. Results and discussions are provided in Section 5, with conclusions drawn in Section 6.

## 2. Coordinative merging control strategy for mixed traffic (M-CoMC)

The Coordinative Merging Control for Mixed-traffic strategy, called M-CoMC, is developed based on the Coordinative Merging Control (CoMC) strategy for full CAV contexts in Zhu et al. [28]. As illustrated in Fig. 1, the strategy is composed of three components: (1) mainline vehicles proactively decelerate to create large merging gaps on the mainline freeway; (2) ramp vehicles stop on the ramp and form proper platoons before entering the main road; (3) the created mainline gaps and the formed ramp platoons are coordinated by a control center in terms of size, speed, and arrival time. To ensure the efficiency and smoothness of merging, three requirements should be satisfied through the centralized coordination: (1) the created mainline gap is large enough to accommodate the merging platoon (size requirement); (2) the facilitating vehicle and the merging platoon reach the same speed at the merging point (speed requirement); and (3) when the merging platoon arrives, the gap is just available at the merging point (arrival time requirement). It should be noted that the key difference between our proposed coordination compared to existing studies is that we aim to optimize the overall traffic efficiency at the continuous traffic flow level rather than

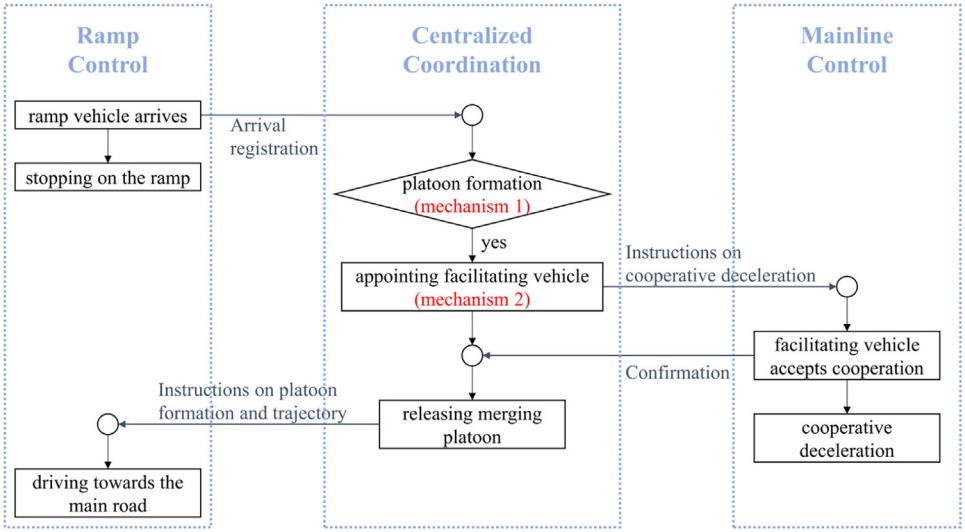


**Fig. 1. M-CoMC strategy** [28].

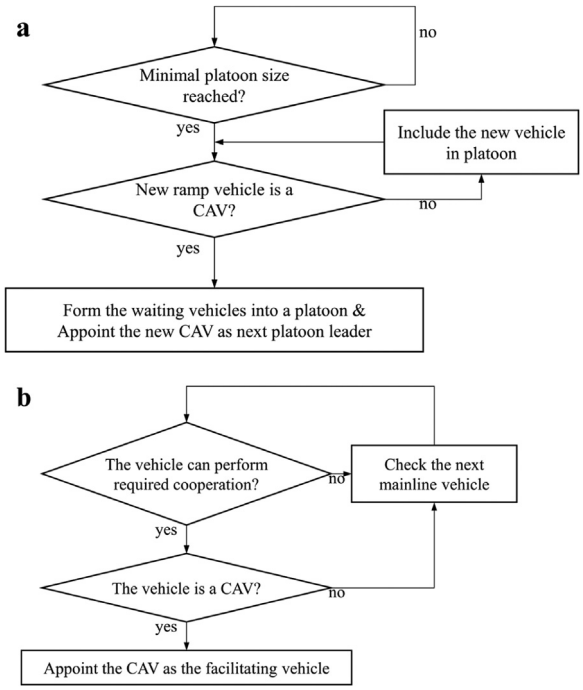


**Fig. 2. Decision mechanisms.** (a) Formation of merging platoon. (b) Appointment of facilitating vehicle.

the local traffic efficiency of a ramp platoon and several vehicles in the mainline.

Under such a system, the coordination instructions from the control center are only sent to the facilitating vehicle on the main road and the platoon leader on the ramp, while the other vehicles follow their preceding vehicles in accordance with the regular car-following rules. That means that only some CAVs are controlled and other vehicles (e.g., HDVs) are not controlled by the proposed strategy. Essentially, such a coordination system uses CAVs as actuators to regulate the behaviors of surrounding HDVs. For example, if we do not consider the option of free lane-changing, when a preceding CAV decelerates or stops, the HDVs following this CAV are forced to decelerate or stop. In this way, the HDVs are indirectly controlled and incorporated into the coordination system. Therefore, it is only necessary to ensure that the facilitating vehicle and the platoon leader in each merging cycle are CAVs, while other vehicles (e.g., platoon followers, mainline vehicles following the facilitating vehicle) can be HDVs driving in their regular manner.

In order to ensure that the merging platoon leader and the mainline facilitating vehicle in each merging cycle are CAVs, two mechanisms are developed to determine the formation of the merging platoon and the appointment of facilitating vehicle.

Decision mechanism 1: formation of merging platoon

As shown in Fig. 2a, the formation of a merging platoon should satisfy two conditions: (1) enough vehicles are accumulated on the ramp, and (2) the next vehicle directly after the platoon is a CAV. The decision mechanism is triggered every time a new ramp vehicle arrives. The control center first counts the number of vehicles waiting on the ramp (excluding the new vehicle). If the minimum number is reached, the control center further checks if the new vehicle is a CAV. If yes, the waiting vehicles are grouped as a platoon, and the new CAV is appointed as the leader of the next platoon. This ensures that the first vehicle in a platoon (i.e., the platoon leader) is always a CAV.

Decision mechanism 2: appointment of mainline facilitating vehicle

According to the decision mechanism in Fig. 2b, the mainline vehicle appointed as the facilitating vehicle should satisfy two conditions: (1) it is able to perform the required cooperation, that is, the vehicle has not reached the required speed-change position when being appointed; and (2) the vehicle is a CAV. When the coordination is initiated, the control center checks the mainline vehicles one by one (from front to back) and appoints the first vehicle that meets the above two conditions as the facilitating vehicle.

The M-CoMC strategy is formulated under a bi-level coordination framework consisting of macro-level and micro-level coordination decisions, as illustrated in Fig. 3. The macro-level takes traffic state parameters as inputs and uses optimization methods, combined with macroscopic traffic flow models, to determine the minimal platoon size ($n_{min}$) and the cooperative merging speed ($v_C$). According to the mechanism for platoon formation, the actual size of a merging platoon depends on the type of arrived vehicles (i.e., HDV or CAV) and is different for different merging cycles, so the speed-change position of the facilitating vehicles also varies across different cycles. Specifically, the facilitating vehicle decelerates at an earlier position to create a larger gap for a larger platoon and a later position for a smaller platoon. The variations are accommodated at the micro-level, where the outputs from the macro-level and the real-time information about traffic operation are used as inputs to determine the speed-change position ($d$) and the platoon acceleration trajectory ($a$) in each merging cycle. Note that, as long as the

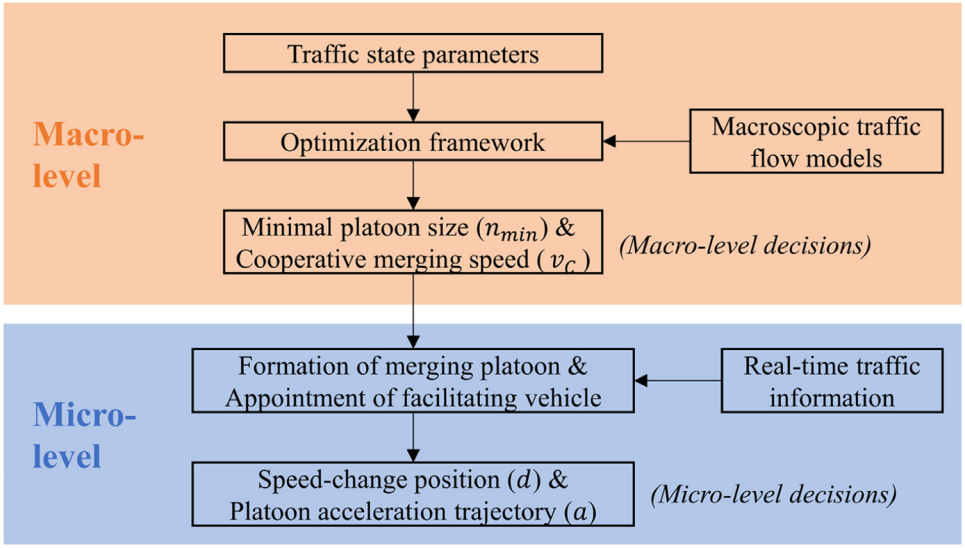


**Fig. 3. Bi-level coordination framework.**

macroscopic traffic state is stable, the macro-level decisions (i.e., $n_{min}$ and $v_C$) remain unchanged across merging cycles, whereas the micro-level decisions (i.e., $d$ and $a$) are updated in each cycle to conform to real-time traffic operation.

Note that, although employing the same concepts of gap creation and platoon merging, this work is significantly different from our previous studies [28,29] in two senses: (1) The previous studies assume a full CAV context, whereas this work tackles at the more challenging conditions of mixed traffic flow with CAVs and HDVs. The presence of HDVs introduces large uncertainties that must be addressed in the coordination at both macro and micro levels. (2) The previous work only employs a macroscopic optimization model for coordination design, whereas the current work enhances coordination by integrating flexible decision mechanisms and micro-level adaptations. Particularly, a receding horizon scheme is embedded at the micro level to accommodate uncertainties of HDVs in terms of arrival patterns and driving behavior. These add-ons will improve the real-time adaptivity of the coordination.

## 3. Bi-level coordination model

Before formulating the bi-level structure, we define in Fig. 4 the important positions: the Merging Point (MP), the End-of-Merge (EM), the mainline Speed-Change (SC) position, and the ramp Waiting Position (WP). Further, we define that all vehicles on the main road that are affected by the cooperative deceleration (including the facilitating vehicle itself) are referred to as cooperative vehicles. The process of one gap creation and one platoon merging is defined as a merging cycle, and M-CoMC functions by running merging cycles recurrently. In one merging cycle, after the controlled on-ramp CAVs merge into the mainline (i.e., the lane-changing maneuver is finished), the control on CAVs will be removed, and all vehicles will drive as per their own driving behavior maneuvered by human drivers and programmed controllers in vehicles. For facilitating vehicles in the mainline in one merging cycle, the coordination controls will be removed after the last vehicle of the ramp platoon merges into the mainline.

### 3.1. Macro-level coordination

At the macro-level, we integrate macroscopic traffic models into an optimization framework to determine the optimal macro-level decisions in accordance with real-time traffic states. Note that the benefits of M-CoMC essentially come from the reallocation of spaces on the mainline freeway, and a theoretical explanation on this point is available in Zhu et al. [28]. By reducing traffic flow speed on the main road, the mainline traffic changes from the original state (state O) to the cooperative state (state C). In comparison with state O, the traffic density and flow rate at state C are higher, thus leaving room for the merging of on-ramp traffic. An essential part of such kind of coordination is that the cooperative deceleration on the main road may cause negative effects on the following mainline traffic, and these effects need to be carefully controlled to ensure that the effect does not persist and accumulate over time.

#### 3.1.1. Merging platoon formation and mainline cooperation

According to decision mechanism 1, when the minimal platoon size is reached, the HDVs that arrive subsequently will still be included in the platoon until a new CAV arrives. Therefore, the size of a merging platoon is determined by the number of HDVs that consecutively arrive after the minimal platoon size is reached:

$$n = n_{min} + n_H \tag{1}$$

where $n$ is the merging platoon size (in number of vehicles), $n_{min}$ is the minimal platoon size, and $n_H$ is the number of consecutive HDVs arriving after $n_{min}$ is reached. We consider each ramp vehicle arrives independently, with a probability $p$ of being a CAV ($p$ equals the penetration rate of CAV in the traffic flow), then the arrival of ramp vehicles is described as an infinite Bernoulli process with constant success probability $p$, where a success represents the arrival of a CAV, and a failure an HDV. In this Bernoulli process, $n_H$ is the number of failures needed to get the first success, which follows a geometric distribution with the probability density function:

$$P(n_H) = (1-p)^{(n_H)} \cdot p,\ n_H \in \{1, 2, 3\ \ldots\} \tag{2}$$

Thus, the merging platoon size follows a shifted geometric design:

$$P(n) = (1-p)^{(n-n_m in)} \cdot p,\ n \in \left\{n_{min},\ n_{min}+1,\ n_{min}+2,\ \ldots\right\} \tag{3}$$

with the expectation

$$\bar{n} = \sum_{n=n_{\min}}^{\infty} n \cdot P(n) = n_{\min} + \frac{1}{p} - 1 \tag{4}$$

The gap size created by the cooperative deceleration and the gap size required for accommodating a merging platoon are given below:

$$G_{created} = h_O + \frac{d}{v_C} - \frac{d}{v_O} \tag{5}$$

$$G_{required} = (n+1)h_C \tag{6}$$

where $v_O$ and $v_C$ are the mainline traffic speed at state O and state C, respectively; $d$ is the distance from SC to MP as in Fig. 4; $h_O$ is the inter-vehicle headway in state O derived from the flow rate $q_O$; and $h_C$ is the car-following headway in state C. Combining (5) and Eq. 6, the SC position (defined by $d$ in Fig. 4) to create the required gap is

$$d = \frac{v_O v_C}{v_O - v_C}\left[(n+1)h_C - h_O\right] \tag{7}$$

The value of $d$ is varying and has the expectation

$$\bar{d} = \sum_{n=n_{min}}^{\infty} d \cdot P(n) = \frac{v_O v_C}{v_O - v_C}\left[(\bar{n}+1)h_C - h_O\right] \tag{8}$$

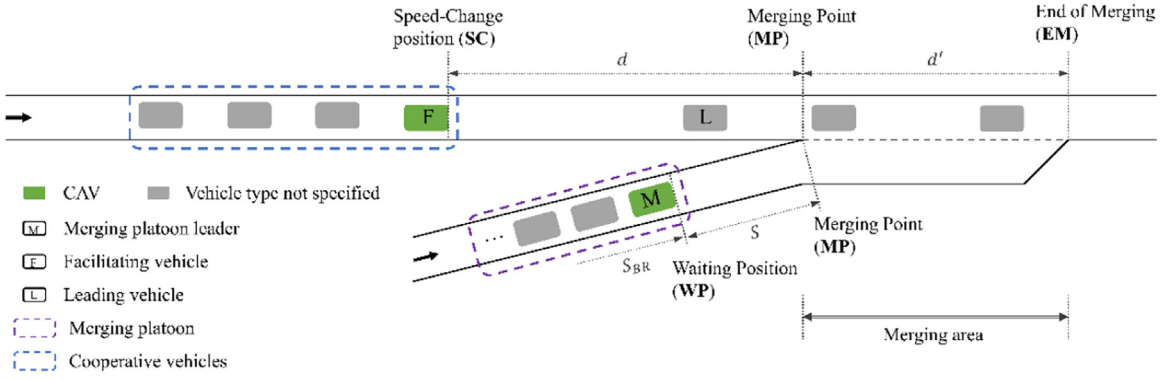


**Fig. 4. Illustration of M-CoMC.**

#### 3.1.2. Cost function

The cost function is explained in detail in Eq. 9. For the sake of text conciseness, in this paper, we do not repeat the detailed derivations in this paper but focus on the architecture and new contents.

To facilitate overall traffic efficiency, the cost is formulated as the total delay to all mainline and ramp vehicles at different weights of mainline and ramp delays.

$$\min D = w_m \cdot D_{main} + w_r \cdot D_{ramp} \tag{9}$$

where $D_{main}$ and $D_{ramp}$ are the total hourly delay to the mainline and ramp vehicles, respectively. $w_m$ and $w_r$ are corresponding weights. We use $w_m = w_r = 1$ in this paper, while the impacts of weight choice are analyzed in detail in Zhu et al. [29].

*3.1.2.1. Mainline delay.* Considering the distribution of $n$, the total mainline delay is estimated as

$$D_{main} = r \cdot \sum_{n=n_{min}}^{N_{max}} P(n) \cdot D^n_{main} \tag{10}$$

$$D^n_{main} = \sum_{i=1}^{m} \left(t^i_M - t_{M0}\right) \tag{11}$$

$$t_{M0} = \frac{d + d'}{v_O} \tag{12}$$

$$t^i_M = \left(1 - \frac{v_O}{v_C}\right) \cdot \frac{(i-1)\omega h_O}{v_O - \omega} + \frac{d + d'}{v_C} \tag{13}$$

$$r = \frac{q_r}{n} \tag{14}$$

with

$$\omega = \frac{q_C - q_O}{k_C - k_O} \tag{15}$$

$$m = \left\lceil \frac{d + d'}{h_O} \times \left(\frac{1}{\omega} - \frac{1}{v_O}\right) \right\rceil \tag{16}$$

Here, $D^n_{main}$ is the mainline delay resulting from the merging of a platoon consisting of $n$ vehicles; $N_{max}$ is the maximal platoon size in reality, which may be very large (even with a low probability) if the penetration rate of CAVs is low; $r$ is the coordination rate defined as the expected number of merging cycles in an hour; $m$ is the number of cooperative vehicles in a merging cycle with a size-$n$ platoon; $t^i_M$ is the travel time of the $i^{\text{th}}$ cooperative vehicle; $t_{M0}$ is the ideal travel time of a mainline vehicle; $d'$ is the distance between MP and EM as in Fig. 4; and $\omega$ is the shockwave speed caused by the transition of traffic state, with $q_O$ and $q_C$ as the flow rates in state O and state C and $k_O$ and $k_C$ as the densities; and $q_r$ is the on-ramp flow rate. $\lceil \cdot \rceil$ in Eq. 16 represents the nearest upper integer.

*3.1.2.2. Ramp delay.* The total ramp delay is estimated as

$$D_{ramp} = r \cdot \sum_{n=n_{min}}^{\infty} P(n) \cdot D^n_{ramp} \tag{17}$$

$$D^n_{ramp} = \sum_{j=1}^{n} \left(t^j_R - t_{R0}\right) \tag{18}$$

$$t^j_R = t^j_{BR} + t^j_{WT} + t^j_{RT} + t^j_{MT} \tag{19}$$

$$t^j_{BR} = \frac{v_r}{b} \tag{20}$$

$$t^j_{WT} = \frac{n - j}{\lambda} \tag{21}$$

$$t^j_{MT} = \frac{d'}{v_C} \tag{22}$$

where $D^n_{ramp}$ is the ramp delay to a merging platoon of $n$ vehicles; $t^j_R$ is the travel time of the $j^{\text{th}}$ vehicle in the platoon; and $t_{R0}$ is the ideal travel time of a ramp vehicle. As in Eq. 19, $t^j_R$ consists of four parts: the barking time before arriving at WP ($t^j_{BR}$), the waiting time at WP ($t^j_{WT}$), the ramp travel time from WP to MP ($t^j_{RT}$), the mainline travel time from MP to EM ($t^j_{MT}$). $t^j_{BR}$, $t^j_{WT}$, and $t^j_{MT}$ are given in Eqs. 20-22, where $v_r$ is the initial arrival speed of ramp vehicles; $b$ is the braking rate; $\lambda$ is the ramp vehicle arriving rate assuming a Poisson distribution with $\lambda = q_r/3600$. Derivations of the above equations are detailed in Zhu et al. [28] and thus not repeated here.

For smooth coordination, we expect that the $j^{\text{th}}$ vehicle in the platoon arrives at the MP $(n + 1 - j)h_C$ seconds earlier than the facilitating vehicle (for example, the platoon leader with $j = 1$ arrives $nh_C$ seconds earlier than the facilitating vehicle), namely

$$t^j_{RT} = t_f - (n + 1 - j)h_C \tag{23}$$

where $t_f$ is the time it takes for the facilitating vehicle to arrive at the MP. According to decision mechanism 2, the facilitating vehicle is the first CAV behind the SC. As shown in Fig. 5, we consider the presence of CAVs in mainline traffic as an infinite Bernoulli process, where each trial has a probability $p$ of being a success (indicating a vehicle is a CAV). The number of trials (vehicles) to get the first success (CAV) follows a shifted geometric distribution with the expectation $1/p$. That is, it is expected that the facilitating vehicle is the $1/p^{\text{th}}$ vehicle behind SC. Therefore, the expected position ($P_f$) and arrival time of the facilitating vehicle ($t_f$) are

$$\begin{aligned} P_f &= d + \left(\frac{1}{p} - 0.5\right) h_O v_O \\ t_f &= \frac{P_f - d}{v_O} + \frac{d}{v_C} \end{aligned} \tag{24}$$

To ensure that the platoon is able to accelerate to the cooperative speed $v_C$ within the time $t^j_{RT}$, we determine the location of WP (defined by $S$ in Fig. 4) and the estimated acceleration rate ($a$) as

$$S = \frac{v_C t^1_{RT}(n_{min})}{2} \tag{25}$$

$$a = \frac{v_C}{t^1_{RT}(n_{min})} \tag{26}$$

where $t^1_{RT}(n_{min})$ is the ramp travel time of the leader of a size-$n_{min}$ platoon given by (23). Note that the leader of a minimal platoon of size $n_{min}$ is used because this is the most critical case in terms of the required acceleration time. For the other vehicles (e.g., followers in a platoon or vehicles in a larger platoon), $t^j_{RT}$ is longer, so the vehicles can adopt a lower acceleration or depart later.

The original travel time of a ramp vehicle ($t_{R0}$) is given by

$$t_{R0} = \frac{S_{BR} + S}{v_r} + \frac{d'}{v_O} \tag{27}$$

with the ramp braking distance $S_{BR} = \frac{v_r^2}{2b}$.

#### 3.1.3. Constraints

In the macro-level optimization model, the following constraints are applied:

$$\frac{n}{\lambda} \geq \frac{d + d'}{\omega} \tag{28}$$

$$v_{crit} \leq v_C < v_O \tag{29}$$

$$a \leq a_{ramp} \tag{30}$$

$$0 < \bar{n} \leq n_{max},\ n_{min} \in \mathbb{N}^+ \tag{31}$$

$$0 < \bar{d} \leq d_{max} \tag{32}$$

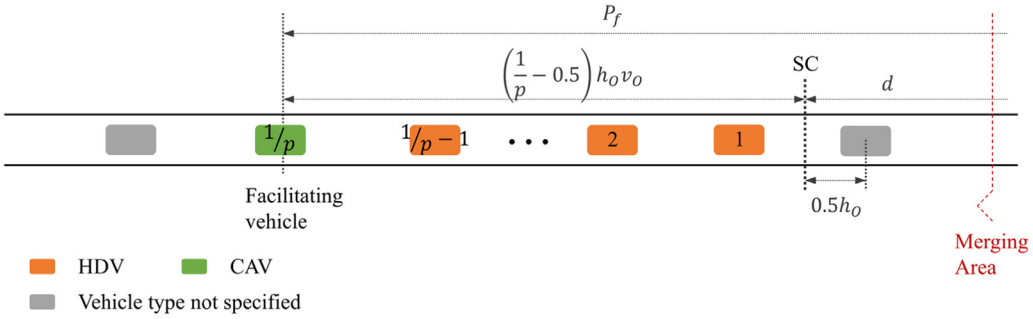


**Fig. 5. Position of facilitating vehicle.**

where $a_{ramp}$ is the maximum ramp acceleration; $n_{max}$ and $d_{max}$ are the upper limits of platoon size and SC position, respectively. Here, constraints (28)-(29) ensure that the cooperation does not break the mainline traffic flow. Constraint (30) specifies the upper limit of ramp acceleration. Constraints Eqs. 31-32 ensure the coordination plan is reasonable for real-world implementation.

In the macro-level optimization problem, we use macroscopic traffic state parameters (e.g., traffic flow rate, speed, CAV penetration rate) as inputs and estimate the expectations of traffic operation patterns in the ramp merging coordination. The model minimizes total delay to all mainline and ramp vehicles by searching for the optimal combination of two coordination variables: minimal merging platoon size ($n_{min}$) and cooperative speed ($v_C$). To ensure feasibility and robustness of the coordination, the optimization is subject to constraints on traffic operation, vehicle dynamics, and real-world implementation needs.

### 3.2. Micro-level coordination

The macro-level employs an optimization model to determine the minimal platoon size ($n_{min}$) and the cooperative speed ($v_C$). Based on the macro-level decisions, the micro-level updates the SC position ($d$) and the platoon trajectory in each merging cycle to accommodate uncertainties and stochastics in real-time traffic operation. Specifically, two aspects are determined by the ongoing traffic:

- The actual size ($n^*$) and composition ($n^*_{CAV}$ and $n^*_{HDV}$, with $n^*_{CAV} + n^*_{HDV} = n^*$) of a merging platoon.
- The actual positions of the appointed facilitating vehicle and its original leader of the facilitating vehicle in the mainline ($P^*_f$, $P^*_l$).

The size and composition of a merging platoon ($n^*_{CAV}$, $n^*_{HDV}$) determine the size of the required merging gap and the position where the facilitating vehicle decelerates ($d^*$). When the platoon consists of more vehicles, especially more HDVs, the facilitating vehicle decelerates at an earlier position to create a larger gap. The actual positions of the facilitating and leading vehicles determine the original gap between them and thereby have an influence on the SC position ($d^*$) and the platoon trajectory ($a^*$). For example, when the original gap is larger, the facilitating vehicle decelerates at a later position and still expands the gap to the required size; in addition, when the leading vehicle is originally closer to the MP, the platoon adopts higher acceleration to catch up with the gap behind it.

#### 3.2.1. Appointment of facilitating vehicle

According to decision mechanism 2, the facilitating vehicle is the first CAV behind the SC. However, the actual SC position is related to the original position of facilitating vehicle, as explained above. To solve this endogenous problem, we adopt a traversal approach at the micro-level to appoint the facilitating vehicle, as shown in Fig. 6.

We consider a mainline CAV, $k$, and its leader, $k-1$, and assume that their position and speed information are available through on-board

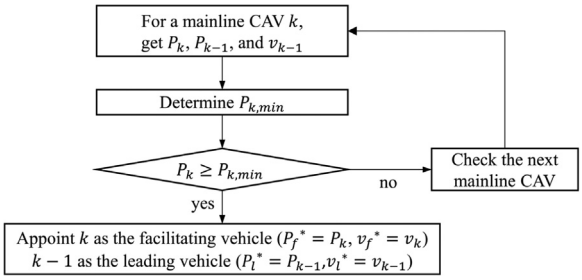


**Fig. 6. Traversal approach to appoint the facilitating vehicle.**

sensors and communication systems. Then, the CAV $k$ must meet two conditions to be the facilitating vehicle:

- Condition 1: it should be able to create enough gap from the vehicle $k-1$, i.e.,

$$\frac{P_k}{v_C} - \frac{P_{k-1}}{v_{k-1}} \geq \left(n^*_{CAV}+1\right) \cdot h_C^{CAV} + n^*_{HDV} \cdot h_C^{HDV} \tag{33}$$

where $P_k$ and $P_{k-1}$ are the positions of the vehicles $k$ and $k-1$, respectively, defined by their distances to the MP; $v_{k-1}$ is the speed of $k-1$; $n^*_{CAV}$ and $n^*_{HDV}$ are the actual number of CAVs and HDVs in the merging platoon; $h_C^{CAV}$ and $h_C^{HDV}$ are the car-following headways of CAVs and HDVs at the speed $v_C$. The distance between the last vehicle in the platoon and vehicle $k$ is $h_C^{CAV}$ because $k$ is a CAV.

- *Condition 2*: it should be able to create enough gap from the platoon leader, i.e.,

$$\frac{P_k}{v_C} - t_{RT,min} \geq n^*_{CAV} \cdot h_C^{CAV} + n^*_{HDV} \cdot h_C^{HDV} \tag{34}$$

where $t_{RT,min}$ is the minimal time needed for the platoon leader to arrive at the MP, given its waiting position and acceleration capability:

$$t_{RT,min} = \frac{v_C}{a_{max}} + \frac{S - \frac{v_C^2}{2a_{max}}}{v_C} = \frac{S}{v_C} + \frac{v_C}{2a_{max}} \tag{35}$$

where $a_{max}$ is the maximum comfortable acceleration that the ramp vehicles adopt and set to be 2 m/s$^2$. The two conditions are considered separately, because when the vehicle $k-1$ is originally close to the MP, there is a possibility that the platoon cannot catch up with $k-1$ at a headway of $h_C^{CAV}$, even though it travels at the maximum acceleration. In this case, a larger gap is needed to accommodate the extra distance between the platoon and the leading vehicle. Combining Eqs. (33)-(34), we obtain the foremost position for the vehicle $k$ to be the facilitating vehicle ($P_{k,min}$):

$$P_{k,min} = \max \left\{ \begin{matrix} \frac{P_{k-1} v_C}{v_{k-1}} + \left[\left(n^*_{CAV}+1\right)h_C^{CAV} + n^*_{HDV} h_C^{HDV}\right] v_C \\ t_{RT,min} v_C + \left[n^*_{CAV} h_C^{CAV} + n^*_{HDV} h_C^{HDV}\right] v_C \end{matrix} \right\} \tag{36}$$

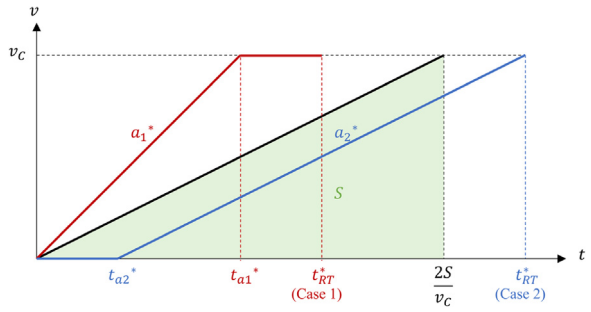


**Fig. 7. Trajectory of platoon leader.**

If the actual position of $k$ is farther than $P_{k,min}$, vehicle $k$ is qualified to be the facilitating vehicle. To appoint the facilitating vehicle, the mainline CAVs are checked one by one from front to back until the first CAV that satisfies $P_k \geq P_{k,min}$ is found.

### 3.2.2. Speed-change position

In the coordination, the facilitating vehicle is expected to arrive at the MP $n_{CAV}^* h_C^{CAV} + n_{HDV}^* h_C^{HDV}$ later than the platoon leader, namely

$$t_f^* = t_{RT}^* + n_{CAV}^* h_C^{CAV} + n_{HDV}^* h_C^{HDV} \tag{37}$$

where $t_f^*$ is the arrival time of the facilitating vehicle, and $t_{RT}^*$ is the actual ramp travel time of the platoon leader determined by

$$t_{RT}^* = \max\left\{ \frac{P_l^*}{v_l^*} + h_C^{CAV}, t_{RT,min} \right\} \tag{38}$$

where $P_l^*$ and $v_l^*$ are the position and speed of the leading vehicle. Consider that the facilitating vehicle keeps its original speed $v_f^*$ before arriving at the SC and decelerates to $v_C$ afterwards, the vehicle arrives the MP at

$$t_f^* = \frac{P_f^* - d^*}{v_f^*} + \frac{d^*}{v_C} \tag{39}$$

where $P_f^*$ is the position of the facilitating vehicle, and $d^*$ is the distance between SC and MP. Combining (37) and (39) gives the actual SC position (defined by the distance to the MP, $d^*$):

$$d^* = \frac{v_f^* v_C}{v_f^* - v_C}\left( t_{RT}^* + n_{CAV}^* h_C^{CAV} + n_{HDV}^* h_C^{HDV} - \frac{P_f^*}{v_f^*} \right) \tag{40}$$

### 3.2.3. Platoon acceleration trajectory

As discussed above, the required ramp travel time of the merging platoon ($t_{RT}^*$) depends on ongoing traffic operation in each merging cycle. Therefore, the acceleration trajectory of the platoon leader is adapted for each merging cycle. This paper focuses on the bi-level M-CoMC strategy instead of the lower-level CAV trajectory design. Indeed, the design of CAV merging trajectories is formulated as a separate research problem and has been extensively visited by recent research [10,13,16]. Therefore, we do not dig deep into complicated trajectory methods in this paper but use a quick solution to complete the proposed M-CoMC coordination. In practice, it is possible to embed a more sophisticated lower-level trajectory planner into M-CoMC, such as Ward et al. [30] and Malikopoulos [16].

Our example trajectory planner uses a constant ramp acceleration rate. As shown in Fig. 7, the time needed for a vehicle to constantly accelerate from stopping to $v_C$ within the distance $S$ is $\frac{2S}{v_C}$ (black solid line in Fig. 7). Depending on the relationship between $\frac{2S}{v_C}$ and the required ramp travel time $t_{RT}^*$, two cases are distinguished: $t_{RT}^* \leq \frac{2S}{v_C}$ and $t_{RT}^* > \frac{2S}{v_C}$. When $t_{RT}^* \leq \frac{2S}{v_C}$ (red case in Fig. 7), we require the vehicle to first accelerate at a higher rate $a_1^*$ until reaching $v_C$ and then keep $v_C$ until arriving at the MP. The acceleration time ($t_{a1}^*$) and rate ($a_1^*$) are

$$t_{a1}^* = \frac{2\left(v_C t_{RT}^* - S\right)}{v_C} \tag{41}$$

$$a_1^* = \frac{v_C^2}{2\left(v_C t_{RT}^* - S\right)} \tag{42}$$

When $t_{RT}^* > \frac{2S}{v_C}$ (blue case in Fig. 7), the vehicle departs later to extend the travel time on the ramp. The departure time ($t_{a2}^*$) and acceleration rate ($a_2^*$) in this case are:

$$t_{a2}^* = t_{RT}^* - \frac{2S}{v_C} \tag{43}$$

$$a_2^* = \frac{v_C^2}{2S} \tag{44}$$

### 3.2.4. Receding horizon scheme

Once the facilitating vehicle, speed-change position and platoon acceleration trajectory are determined and planned, the local coordination will be executed by controlling the speed of facilitating vehicle in the mainline and the leader of the ramp platoon in time series. When implementing the proposed micro-level coordination, there are some uncertain dynamics that cannot be fully controlled due to the existence of human drivers. For instance, the HDVs in ramp platoons do not reach steady car-following headways in Eqs. (36)-(43) before merging due to human reaction time and variances in real driving behavior; the leading vehicle in mainline (Fig. 4c) slows down due to some unexpected events (e.g., calling on mobile phones). These uncertainties and unexpected events during executing micro-layer coordination may result in the failure of platoon merging as they will change the arrival time of mainline facilitating vehicles and the leading and last vehicles of the ramp platoon at the merging point. To accommodate such uncertainties, we embed a Receding Horizon Control scheme in micro-layer coordination after the merging process is initiated in a certain merging cycle. More specifically, the control variables in Sections 3.2.2 and 3.2.3 are recalculated and updated in a specific control step, namely the equations in Sections 3.2.2 and 3.2.3. The control is subject to the constraints demonstrated in Eqs. (40)-(46). In a specific coordination cycle, the facilitating vehicle in the mainline will not change. Therefore, the Receding Horizon Control is realized by updating control variables, including acceleration of the facilitating vehicle in the mainline and the leader of the ramp platoon at every control time step. The overall control horizons for facilitating vehicle in the mainline and the leading vehicle ramp platoon is the time from SC to MP and the distance from WP to MP as shown in Fig. 4. The control variables are updated every 1 second, which is the length of each step. The details of the receding horizon control scheme are described in Table 1.

## 4. Simulation-based performance analysis

### 4.1. Simulation establishment

We utilize a combination of the SUMO simulator and Python program to evaluate the performance of the proposed control strategy. The proposed two-level control strategy is programmed in Python and interacts with the SUMO via Traffic Control Interface (TraCI) [31], where real-time traffic information (e.g., position, speed, and acceleration of vehicles) is passed from SUMO to Python as inputs of the micro-level models in Section 3.2, and the micro-level coordination decisions are determined in Python and then fed back to SUMO for real-time coordination in the simulation environment.

A merging segment in the freeways of Shanghai, China (see Fig. 10) based on real road configurations was simulated in SUMO. The merging

**Table 1**
**Driving behavior model parameters.**

Receding Horizon Scheme

Control objective: $J = \text{Min} \sum_i^N (|t_f^i - (t_{RT}^{*,i} + n_{CAV}^* h_C^{CAV} + n_{HDV}^* h_C^{HDV})| + |t_{rl}^i - t_{RT}^{*,i}|)$

$$t_{RT}^{*,i} = \max\{\frac{s_l^i}{v_l^i} + h_C^{CAV}, t_{rl}^i\}$$

Control variables: $a_f^i$, $a_{rl}^i$
Constraints: $b_{max} < a_f^i$, $a_{rl}^i < a_{max}$, Eqs. (40)-(46)
where:
$b_{max}$, $a_{max}$: The maximum deceleration (−3 m/s$^2$) and acceleration (2 m/s$^2$) of vehicles.
$t_f^i$, $t_{rl}^i$ : The predicted arrival timing at the MP of mainline facilitating vehicle and ramp platoon leading vehicle at the $i^{\text{th}}$ step.
$a_f^i$, $a_{rl}^i$: The acceleration of mainline facilitating vehicle and ramp platoon leading vehicle at the $i^{\text{th}}$ step.
$s_f^i$, $s_{rl}^i$ : The distance of mainline facilitating vehicle and ramp platoon leading vehicle to MP at the $i^{\text{th}}$ step. If the facilitating vehicle or ramp platoon leading vehicle passes the MP, $s_f$ or $s_{rl}$ will be set to zero, respectively.
$v_f^i$, $v_{rl}^i$ : The real-time speed of mainline facilitating vehicle and ramp platoon leading vehicle to MP at the $i^{\text{th}}$ step.
$v_l^i$, $s_l^i$: The speed and distance to MP of the preceding vehicle before the mainline facilitating vehicle at the $i^{\text{th}}$ step.
$v_{re}^i$, $s_{re}^i$, $a_{re}^i$: The speed, distance to MP and acceleration of the last vehicle of the ramp platoon.
$\Delta t$: Update step, 1 s.
**While** $s_{rl}^i > 0$ or $s_f^i > 0$ **do**
  Collect or update $a_f^i$, $a_{rl}^i$, $s_f^i$, $s_{rl}^i$, $v_f^i$, $v_{rl}^i$, $v_l^i$, $s_l^i$
  **If** $s_{rl}^i > 0$ **do**
    **If** $a_{rl}^i > 0.1$ **do**
      $t_{rl}^i = \frac{v_c - v_{rl}^i}{a_{rl}^i} + \frac{s_{rl}^i - (\frac{v_c - v_{rl}^i}{a_{rl}^i} \times \frac{v_c + v_{rl}^i}{2})}{v_c}$
    **Else** $t_{rl}^i = \frac{s_{rl}^i}{v_{rl}^i}$
    **If** $t_{RT}^{*,i} > t_{rl}^i$ **do**
      Use Eqs. (41)-(42) with an initial speed of $v_{rl}^i$ to update $a_{rl}^i$ and final speed of the ramp platoon leading vehicle at MP $v_{rl}^{MP}$
    Update $t_f^i = \frac{s_f^i}{v_f^i}$
    **If** $t_f^i < (t_{RT}^{*,i} + n_{CAV}^* h_C^{CAV} + n_{HDV}^* h_C^{HDV})$ **do**
      Calculate $a_f^i = \frac{v_f^i - \frac{s_f^i}{(t_{RT}^{*,i} + n_{CAV}^* h_C^{CAV} + n_{HDV}^* h_C^{HDV})}}{\Delta t}$
  **If** $s_{rl}^i > 0$ and $s_{rl}^i = 0$ **do**
    Collect $v_{re}^i$, $s_{re}^i$, $a_{re}^i$
    **If** $a_{re}^i > 0.1$ **do**
      Calculate $t_{re}^i = \frac{v_{rl}^{MP} - v_{re}^i}{a_{re}^i} + \frac{s_{re}^i - (\frac{v_{rl}^{MP} - v_{re}^i}{a_{re}^i} \times \frac{v_{rl}^{MP} + v_{re}^i}{2})}{v_{rl}^{MP}}$
    **Else** $t_{re}^i = \frac{s_{re}^i}{v_{re}^i}$
    Update $t_f^i = \frac{s_f^i}{v_f^i}$
    **If** $t_f^i < t_{re}^i + h_C^{HDV}$ **do**
      Calculate $a_f^i = \frac{v_f^i - \frac{s_f^i}{t_{re}^i + h_C^{HDV}}}{\Delta t}$
  Update $i \rightarrow i + 1$

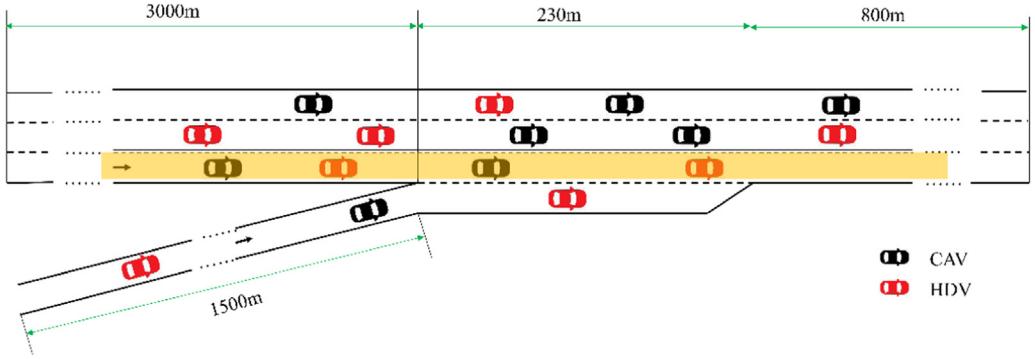


**Fig. 8. Configuration of the simulation road segment.**

area consists of a single-lane on-ramp and a mainline freeway with three lanes. We consider that lane-changing behaviors to the outermost lane are prohibited in and near the merging area on the main road (the area marked in yellow in Fig. 8). This is consistent with traffic regulations in Shanghai and literature [25,32]. The length of the acceleration lane is 230 m. The lane width is 3.5 m. The road segments of 3000 m before and 800 m after the acceleration lane are considered to guarantee stable traffic flow entering control areas and to reflect the impacts of ramp mering on mainline traffic fully. Speed limits for the mainline (including the acceleration lane) and the ramp are 120 km/h and 60 km/h, respectively.

### 4.2. Driving behavior modeling and fundamental diagram

The car-following and lane-changing models are defined in SUMO to reflect realistic driving behavior and traffic flow characteristics in

**Table 2**
**Driving behavior model parameters**.

(a) IDM parameters

| Parameter | HDV | CAV | Unit |
|---|---|---|---|
| $a_{max}$ | 2 | 2 | m/s$^2$ |
| $b_{comf}$ | 3 | 3 | m/s$^2$ |
| $\delta$ | 4 | 4 | – |
| $v_0$ | 120 | 120 | km/h |
| $s_0$ | 1.5 | 1.5 | m |
| $T$ | 1 | 0.6 | s |
| $\tau$ | 1 | 0.1 | s |

(b) Lane-changing parameters

| Parameter | Definition | HDV | CAV | Unit |
|---|---|---|---|---|
| Desired headway | default | 1 | 0.6 | s |
| lcAssertive | Willingness to accept lower front and rear headway on the target lane. The required minimum headway for lane changing is divided by this value, i.e., Minimal accepted lane-changing gap = Desired headway/lcAssertive | 0.8 (5%)<br>1 (20%)<br>1.5 (15%)<br>2 (10%)<br>2.5 (10%)<br>3 (10%)<br>3.5 (10%)<br>4 (10%)<br>4.5 (5%)<br>5 (5%) | 1 (60%)<br>2 (20%)<br>3 (20%) | – |
| lcCooperative | Willingness for performing cooperative lane changing. Lower values result in reduced cooperation. | 1 (25%)<br>0.8 (50%)<br>0.5 (25%) | 1 (25%)<br>0.8 (50%)<br>0.5 (25%) | – |
| lcTimeToImpatience | Time to reach maximum impatience. Impatience grows whenever a lane-change maneuver is blocked. | 180 | Infinity (default, no impatience growth) | s |
| lcImpatience | The dynamic factor for modifying lcAssertive. If the lane-changing maneuver is blocked, the impatience increase with time until successful lane changes | 1 | 0 | – |

the ramp merging area. In this case study, we use the Intelligent Driver Model (IDM) [33–36] to describe the simulated car-following behaviors:

$$\dot{v}(t+\tau) = a_{max}\left[1 - \left(\frac{v(t)}{v_0}\right)^{\delta} - \left(\frac{s_0 + v(t)T + \frac{v(t)\cdot\Delta v(t)}{2\sqrt{a_{max}b_{comf}}}}{s(t)}\right)^2\right] \tag{45}$$

Here, $a_{max}$ is the maximum acceleration, $v_0$ is the desired speed, $\Delta v$ is the relative speed between a vehicle and its leader, $\delta$ is the acceleration exponent, $t$ is time index, $\tau$ is reaction time, $s$ is the net (bumper-to-bumper) spacing, $s_0$ is the standstill (net) spacing, $T$ is the safe time headway, and $b_{comf}$ is the comfortable deceleration. The fundamental diagram of IDM-compliant traffic flow is derived from the steady-following state between vehicles, namely when all vehicles are following at the same constant speed, i.e., $\dot{v} = 0$ and $\Delta v = 0$. Then we have from (45) the condition for the steady following:

$$1 - \left(\frac{v}{v_0}\right)^{\delta} - \left(\frac{s_0 + vT}{s}\right)^2 = 0 \tag{46}$$

where $s = hv - L$, where $h$ is the following headway, and $L$ is the vehicle length. This leads to the headway-speed relationship:

$$h = \frac{s_0 + vT}{v\sqrt{1 - \left(\frac{v}{v_0}\right)^{\delta}}} + \frac{L}{v} \tag{47}$$

In a mixed traffic flow, different IDM parameters are adopted for HDVs and CAVs to reflect their divergent car-following driving behaviors, as in Table 2. **Driving behavior model parameters**. Thus, the headway-speed relationship of a mixed flow is

$$h = ph^{CAV} + (1-p)h^{HDV} \tag{48}$$

where $h^{CAV}$ and $h^{HDV}$ are the steady following headways of CAVs and HDVs, respectively. The fundamental relationships for a mixed flow are then determined with $q = 1/h$ and $k = q/v$. The IDM parameters for this case study are presented in Table 2. The HDV parameters refer to calibrations on empirical trajectory data [37,38]. We adopt 0.6 s safety time headway and 0.2 s reaction time for CAVs, which are in line with Zhou et al. [39] and Durrani et al. [40].

The lane-changing behaviors are modeled by the latest SL2015 model in SUMO [41], and the parameters are summarized in Table 2. In the simulation, we divide each lane into five sub-lanes, each of which has a width of 0.7 m. More importantly, we consider heterogeneity in lane-changing behavior (especially for HDV) to mimic more realistic merging behavior, which has been heavily overlooked in the relevant literature. A key parameter for lane changing is the minimum accepted safety headway (MASH) between a lane-changing vehicle and its putative follower and leader in the target lane. Significant differences among different drivers exist [42–44 and affect the reality of simulated on-ramp merging behavior under no control noticeably. This is realized by setting a distribution of “lcAssertive” parameters for HDV to resemble the empirically calibrated distributions of accepted rear and front headways during lane changing in recognized literature. Furthermore, we also set different “lcAssertive” parameters for CAV to consider potential divergent lane-changing behavior of different CAVs on account that the pre-programmed lane-changing control algorithms of different vehicle manufacturers may be distinct. Moreover, we consider heterogeneous willingness for performing cooperative lane changing among different human drivers [45] by setting “lcCooperative” parameter to be a distribution instead of a constant. Meanwhile, we also consider the impatience of human drivers when the lane-changing maneuver is blocked by setting two parameters “lcImpatience” and “lcTimeToImpatience”. Other lane-changing behavior parameters are default values of SL2015 in SUMO [46].

### 4.3. Study scenarios

In this study, we test the performance of the proposed M-CoMC strategy under various combinations of mainline volumes, on-ramp volumes,

**Table 3**
**M-CoMC input parameters.**

| Parameter | Value | Unit |
|---|---|---|
| $w_m$ | 1 | – |
| $w_r$ | 1 | – |
| $v_O$ | 120 | km/h |
| $v_r$ | 60 | km/h |
| $v_{crit}$ | 75 | km/h |
| $d'$ | 230 | m |
| $a_{ramp}$ | 2.75 | m/s$^2$ |
| $b$ | 2.75 | m/s$^2$ |
| $L$ | 4.37 | m |
| $n_{max}$ | 20 | veh |
| $d_{max}$ | 1500 | m |

and penetration rates of CAV. As the main benefit of M-CoMC is to stabilize traffic and improve merging operation under dense traffic, we focus on the high traffic volume scenarios and consider two levels of mainline flow (1,800 and 2,000 veh/h/lane), three levels of ramp flow (500, 600, and 700 veh/h/lane), and four CAV penetration rates (0.3, 0.5, 0.7, and 0.9). In total, 18 pairs of scenarios (under no controls and with controls) are investigated for comprehensive analysis using the input parameters in Table 3. For each scenario, an M-CoMC control case is simulated and compared to a base case without any traffic controls. The study scenarios and the corresponding M-CoMC macro-level decisions are summarized in Table 4. Note that when CAV penetration is low, the macro-level coordination model has no feasible solution under the most critical traffic volumes, and thus the M-CoMC strategy should not be applied in such scenarios. Meanwhile, when traffic volumes in the mainline and ramp are not large (e.g., the merging frequency of ramp vehicles is not high), it is not necessary to implement the proposed coordination as well. The theoretical reason is that the merging of on-ramp vehicles will not result in significant impacts on the mainline when the traffic volumes in the mainline and ramp are not large. In this case, local coordination among a small platoon on ramp and several vehicles in the mainline is efficient enough, as shockwaves in the mainline caused by on-ramp vehicles merging will not accumulate. Therefore, our proposed coordination is targeted at the critical scenario with large traffic volumes in the mainline and ramps and will be implemented after certain thresholds.

Traffic flows with stochastic arrival patterns are generated using the "duarouter" randomization tool in SUMO. The simulation time step is set to 0.2 s. For each scenario, we repeated the simulation five times with different random seeds. The outputs of the simulation include the location, speed, and acceleration profile of each vehicle. We record information about vehicle positions and speeds in the road segments from 1500 m (mainline) or 1000 m (ramp) upstream of the merging area to 500 m downstream of the merging area. This range covers the merge influence area defined by TRB [47].

## 5. Results and discussion

### 5.1. Performance in reducing traffic oscillation

We first compare the vehicle trajectories under control and base (i.e. no-control) scenarios. We select one typical scenario for demonstration herein. Fig. 9 shows 10-minute vehicle trajectories in the congested scenario 2,000–700–0.7 (mainline volume-ramp volume-penetration rate). In the base case without control (Fig. 9a), the merging of ramp vehicles interferes with mainline traffic and induces stop-and-go behaviors of vehicles on the main road, which result in traffic oscillations of mainline vehicles and intermittent cut-in behaviors of ramp vehicles. These obviously hamper the traffic efficiency and safety in the merging areas. When M-CoMC is in place (Fig. 9b), vehicle trajectories of mainline vehicles are significantly smoothened thanks to the coordination between gap creations in mainline and ramp platoon merging. The proposed control strategy eliminates traffic oscillations in the mainline and enables the smooth merging of the ramp platoon. Taking a specific merging cycle for example (green rectangle in Fig. 9b), a facilitating vehicle in the mainline decelerates to a certain speed at around 1,150 m upstream before the merging point to create gaps that well accommodate the merging platoon (trajectory in yellow and red colors). The cooperative behavior induces a temporary disturbance on the following mainline traffic, which tapers off and eventually dissipates within two minutes without accumulating to the next merging cycle. It is worth noting that the speed-change points of mainline facilitating vehicles and the tra-

**Table 4**
**Study scenarios and M-CoMC macro-level decisions.**

| | | | | | | | | |
|---|---|---|---|---|---|---|---|---|
| (a) CAV penetration $p = 0.3$ | | | | | | | | |
| Traffic volume | $q_m$ | 1800 | 1800 | 1800 | 2000 | 2000 | 2000 | veh/h/lane |
| | $q_r$ | 500 | 600 | 700 | 500 | 600 | 700 | veh/h/lane |
| M-CoMC decision | $n$ | 6 | N/A | N/A | 15 | N/A | N/A | km/h |
| | $v_C$ $v_C$ | 75.5 | | | 75.0 | | | veh |
| (b) CAV penetration $p = 0.5$ | | | | | | | | |
| Traffic volume | $q_m$ | 1800 | 1800 | 1800 | 2000 | 2000 | 2000 | veh/h/lane |
| | $q_r$ | 500 | 600 | 700 | 500 | 600 | 700 | veh/h/lane |
| M-CoMC decision | $n$ | 6 | 10 | N/A | 7 | 19 | N/A | km/h |
| | $v_C$ $v_C$ | 84.0 | 76.5 | | 75.2 | 75.1 | | veh |
| (c) CAV penetration $p = 0.7$ | | | | | | | | |
| Traffic volume | $q_m$ | 1800 | 1800 | 1800 | 2000 | 2000 | 2000 | veh/h/lane |
| | $q_r$ | 500 | 600 | 700 | 500 | 600 | 700 | veh/h/lane |
| M-CoMC decision | $n$ | 6 | 8 | 12 | 7 | 9 | 19 | km/h |
| | $v_C$ $v_C$ | 88.2 | 83.3 | 75.7 | 87.1 | 75.9 | 75.0 | veh |
| (d) CAV penetration $p = 0.9$ | | | | | | | | |
| Traffic volume | $q_m$ | 1800 | 1800 | 1800 | 2000 | 2000 | 2000 | veh/h/lane |
| | $q_r$ | 500 | 600 | 700 | 500 | 600 | 700 | veh/h/lane |
| M-CoMC decision | $n$ | 6 | 7 | 9 | 6 | 8 | 10 | km/h |
| | $v_C$ $v_C$ | 92.0 | 89.0 | 82.2 | 91.8 | 86.2 | 75.7 | veh |

* N/A: not applicable due to low CAV penetration rate.

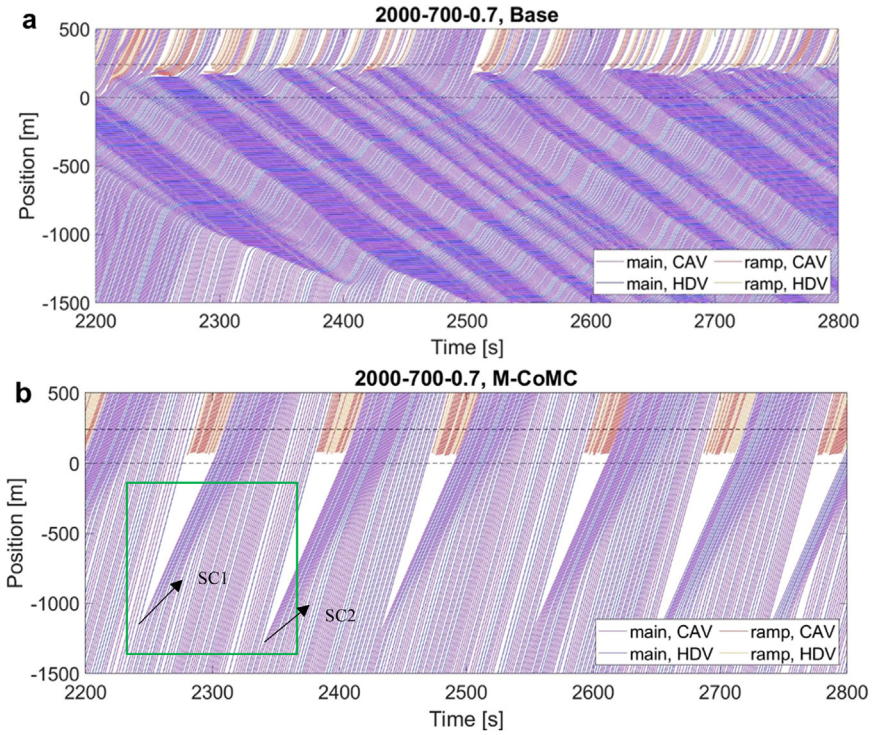


**Fig. 9. Vehicle trajectories (mainline volume 2000 veh/h/lane, ramp volume 700 veh/h/lane, CAV penetration 0.7).** (a)baseline case. (b) M-CoMC case.

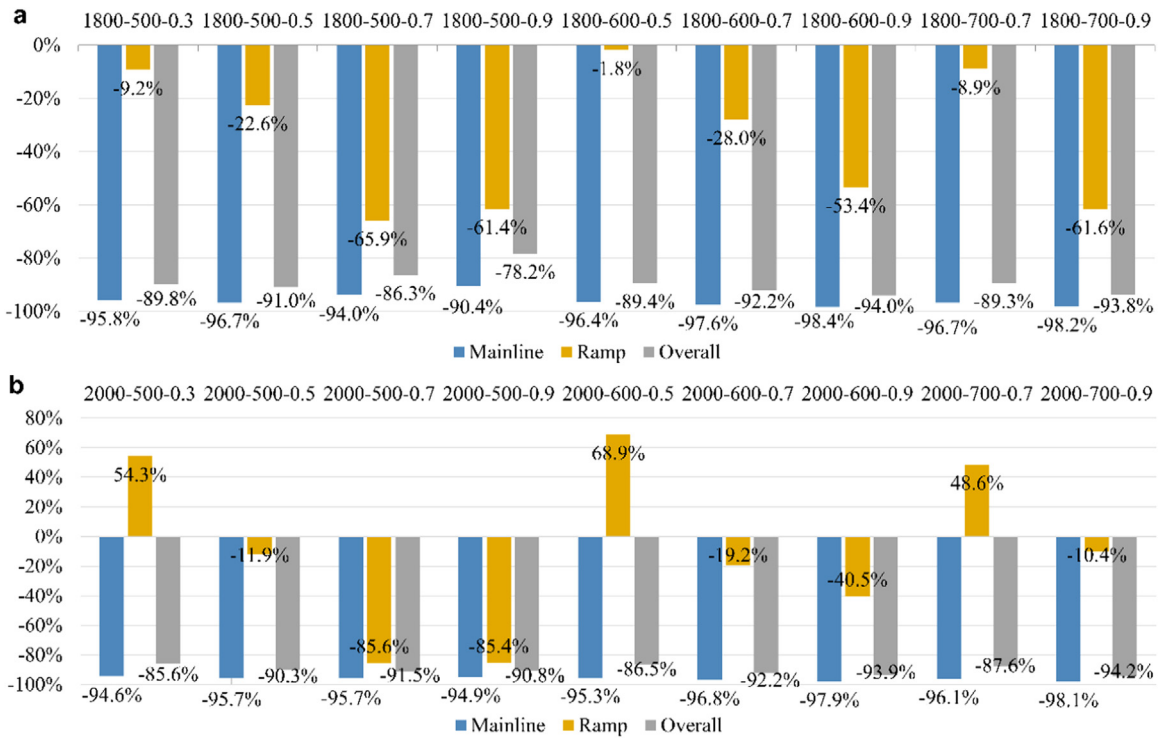


**Fig. 10. Delay reduction resulted from M-CoMC.** (a) 1800 veh/h/lane mainline volume. (b) 2000 veh/h/lane mainline volume.

jectories of merging platoon in different merging cycles are different, e.g., the SC 1 and SC 2 in Fig. 9b. This is attributed to the fact that the sizes of merging platoons in different cycles (notably influencing speed-change point and trajectory of merging platoon) are divergent in the macro-layer control as we consider mixed traffic and stochastic arrival patterns. The results in Fig. 9b indicate that the proposed control strategy can nicely accommodate the arrival stochastics of mixed traffic to guarantee the successful and smooth merging of ramp platoons with different sizes.

### 5.2. Performance in traffic efficiency

Table 5a and Fig. 10a summarize the travel delays of mainline and ramp vehicles to demonstrate the efficiency gains of M-CoMC when the

**Table 5**
**Travel delay results.**

| (a) 1800 veh/h/lane mainline volume | | | | | | | |
|---|---|---|---|---|---|---|---|
| Scenarios(Mainline volume - ramp volume - penetration) | | Average delay (s) | | | Delay reduction (%) | | |
| | | Overall | Main | Ramp | Overall | Main | Ramp |
| 1800–500–0.3 | Base | 215.2 | 265.2 | 67.4 | −89.8% | −95.8% | −9.2% |
| | M-CoMC | 22.0 | 11.0 | 61.2 | | | |
| 1800–500–0.5 | Base | 179.9 | 215.7 | 63.6 | −91.0% | −96.7% | −22.6% |
| | M-CoMC | 16.2 | 7.1 | 49.3 | | | |
| 1800–500–0.7 | Base | 81.3 | 75.5 | 102.4 | −86.3% | −94.0% | −65.9% |
| | M-CoMC | 11.2 | 4.6 | 35.0 | | | |
| 1800–500–0.9 | Base | 38.4 | 28.8 | 74.0 | −78.2% | −90.4% | −61.4% |
| | M-CoMC | 8.4 | 2.8 | 28.5 | | | |
| 1800–600–0.5 | Base | 194.7 | 249.1 | 56.7 | −89.4% | −96.4% | −1.8% |
| | M-CoMC | 20.6 | 9.0 | 55.7 | | | |
| 1800–600–0.7 | Base | 183.8 | 235.4 | 55.6 | −92.2% | −97.6% | −28.0% |
| | M-CoMC | 14.4 | 5.8 | 40.0 | | | |
| 1800–600–0.9 | Base | 167.1 | 208.6 | 63.8 | −94.0% | −98.4% | −53.4% |
| | M-CoMC | 10.0 | 3.4 | 29.7 | | | |
| 1800–700–0.7 | Base | 179.8 | 238.2 | 52.8 | −89.3% | −96.7% | −8.9% |
| | M-CoMC | 19.2 | 7.9 | 48.1 | | | |
| 1800–700–0.9 | Base | 207.0 | 264.3 | 86.5 | −93.8% | −98.2% | −61.6% |
| | M-CoMC | 12.8 | 4.8 | 33.2 | | | |
| Average all scenarios | | | | | −89.3% | −96.0% | −34.7% |
| (b) 2000 veh/h/lane mainline volume | | | | | | | |
| Scenarios (Mainline volume - ramp volume - penetration) | | Average delay (seconds) | | | Delay reduction (%) | | |
| | | Overall | Main | Ramp | Overall | Main | Ramp |
| 2000–500–0.3 | Base | 235.2 | 291.0 | 68.4 | −85.6 | −94.6 | 54.3 |
| | M-CoMC | 33.8 | 15.8 | 105.6 | | | |
| 2000–500–0.5 | Base | 198.0 | 239.8 | 60.4 | −90.3 | −95.7 | −11.9 |
| | M-CoMC | 19.2 | 10.4 | 53.2 | | | |
| 2000–500–0.7 | Base | 163.1 | 145.7 | 297.0 | −91.5 | −95.7 | −85.6 |
| | M-CoMC | 13.8 | 6.3 | 42.8 | | | |
| 2000–500–0.9 | Base | 98.0 | 70.2 | 204.8 | −90.8 | −94.9 | −85.4 |
| | M-CoMC | 9.0 | 3.6 | 29.8 | | | |
| 2000–600–0.5 | Base | 233.1 | 305.3 | 53.7 | −86.5 | −95.3 | 68.9 |
| | M-CoMC | 31.4 | 14.3 | 90.7 | | | |
| 2000–600–0.7 | Base | 210.9 | 267.1 | 53.8 | −92.2 | −96.8 | −19.2 |
| | M-CoMC | 16.4 | 8.4 | 43.5 | | | |
| 2000–600–0.9 | Base | 188.5 | 236.8 | 57.6 | −93.9 | −97.9 | −40.5 |
| | M-CoMC | 11.6 | 4.9 | 34.3 | | | |
| 2000–700–0.7 | Base | 223.1 | 302.8 | 50.3 | −87.6 | −96.1 | 48.6 |
| | M-CoMC | 27.6 | 11.7 | 74.7 | | | |
| 2000–700–0.9 | Base | 251.0 | 356.8 | 41.9 | −94.2 | −98.1 | −10.4 |
| | M-CoMC | 14.6 | 6.8 | 37.5 | | | |
| Average all scenarios | | | | | −90.3% | −96.1% | −9.0% |

mainline volume is 1,800 veh/h/lane. On average, the overall delay of all vehicles is reduced by 89.3% under M-CoMC in comparison to the baseline cases. The travel delays of mainline and ramp vehicles decrease by 96% and 34.7% on average after M-CoMC. These results verify the ability of M-CoMC to significantly improve traffic efficiency in merging areas by eradicating merging conflicts.

When the ramp volume is 500 veh/h/lane, the travel delays of all vehicles under M-CoMC as compared to no-control base cases, reduce by 78.2% - 91%, depending on the penetration rates of CAVs. M-CoMC can simultaneously improve the travel delays of both mainline and ramp vehicles in comparison to base cases. The improvement percentages in travel delays of ramp vehicles increase with penetration rates of CAVs (see Table 5a). The reason is that the travel delays of ramp vehicles under base cases do not change notably with penetration rates, but travel delays of ramp vehicles under M-CoMC reduce signally with penetration rates, as shown in Table 5. The average platoon size in Eq. (4) reduces with increasing penetration rates of CAVs, which means less waiting time to formulate a platoon to discharge. Similar relationships can be observed when ramp volumes are 600 and 700 veh/h/lane. In contrast, improvement percentages in travel delays of mainline vehicles reduce to some extent with larger penetration rates, especially when the penetration rate reaches 0.9. The travel delays of mainline vehicles under M-CoMC merely reduce slightly with increases in penetration rates (see Table 5a). This can also be clearly observed and corroborated in the speed contours of vehicles in Fig. 11. However, the travel delays of mainline vehicles under no controls reduce significantly with penetration rates (see Table 5a and Fig. 11). This reason should be that CAVs have smaller acceptable headways and no reaction time, as described in Section 4.4. These lead to a higher probability of a ramp vehicle merging into a gap between two vehicles without forcing sharp braking of vehicles in the mainline (e.g., fewer traffic oscillations) when the ramp volume is not high (e.g., 500 veh/h/lane). However, Table 5a shows that the improvement percentages in travel delays of mainline vehicles when ramp volumes increase to be 600 and 700 veh/h/lane, are around 92% and do not decrease as notably as they do when the ramp volume is 500 veh/h/lane. The potential explanation is that large ramp volumes result in higher merging frequency and larger probabilities of large merging platoon size (e.g., three vehicles merging successively in a short period).

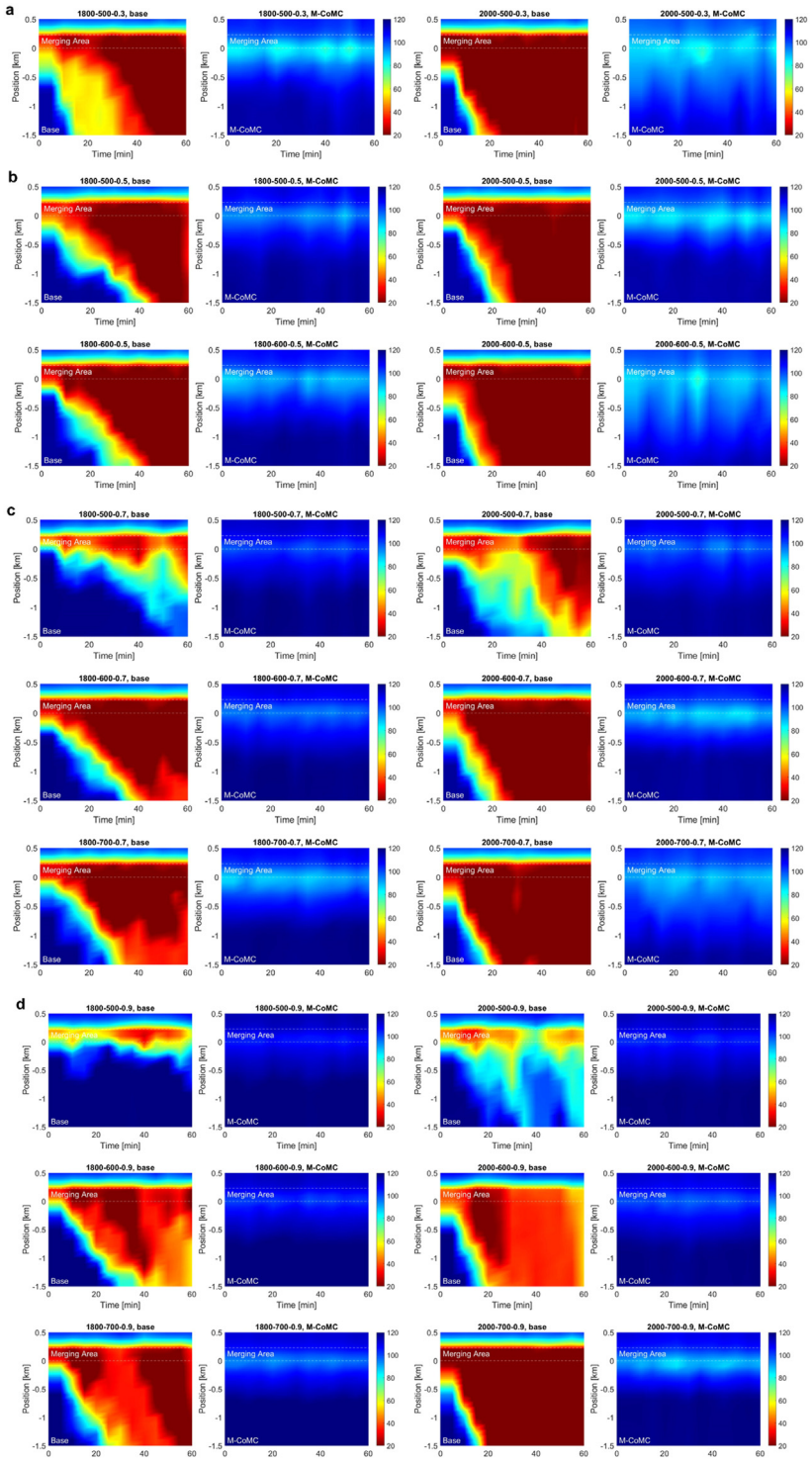


**Fig. 11. Speed contours of mainline traffic.** (a) CAV penetration $p = 0.3$. (b) CAV penetration $p = 0.5$. (c) CAV penetration $p = 0.7$. (d) CAV penetration $p = 0.9$.

Therefore, the merging behaviors of ramp vehicles when ramp volumes are 600 or 700 veh/h/lane, will frequently interrupt the mainline traffic flow and cause oscillations, as demonstrated in Fig. 11, even though high penetration rates of CAVs are beneficial for capacity and merging of one vehicle. Improvements in travel delays of all vehicles when ramp volumes are 600 or 700 veh/h/lane, are in the range of 86.3% - 93.8%. Especially, M-CoMC can substantially reduce travel delays of mainline vehicles by around 96%.

Table 5b and Fig. 10b summarize the travel delays when the mainline volume is 2000 veh/h/lane. The overall travel delays of all vehicles under M-CoMC are improved by 90.3% on average, compared to those in base cases (no-control). The travel delays of mainline and ramp vehicles decrease by 96% and 9% on average. Again, the results validate the capacities of M-CoMC to facilitate traffic efficiency in merging areas. When ramp volume is 500 veh/h/lane and the penetration rate is 0.3, the travel delays of ramp vehicles under M-CoMC actually increase from 68.4 s to 105.6 s by 54.3% in comparison to base cases. The reason is that the average platoon size increases with larger mainline volume and lower penetration rates, as implied by Eq. (4). The larger ramp platoon size means a longer waiting time to formulate a platoon to discharge. So

**Table 6**
**Thresholds of safety surrogate measures.**

| Safety surrogate | Range | Risk level | Symbol | Source |
|---|---|---|---|---|
| TET | 2s < TTC ≤ 5s | low | $TET_{low}$ | Gao et al. [52] |
| | TTC ≤ 2s | high | $TET_{high}$ | |
| MDRAC | 1.7 m/s$^2$ < MDRAC ≤ 3.4 m/s$^2$ | low | $MDRAC_{low}$ | Kuang et al. [50] Arun et al. [53] |
| | MDRAC > 3.4 m/s$^2$ | high | $MDRAC_{high}$ | |
| | Negative MDRAC value * | critical | $MDRAC_{critical}$ | |

* MDRAC is negative when time to collision is less than reaction time (1 second).

**Table 7**
**Rear-end collision risk (mainline volume 2000 veh/h/lane).**

| Scenarios (Mainline volume-ramp volume-penetration) | | $TET_{high}$ (s) | $TET_{low}$ (s) | $MDRAC_{low}$ | $MDRAC_{high}$ | $MDRAC_{critical}$ |
|---|---|---|---|---|---|---|
| 2000–500–0.3 | Base | 38,231.0 | 5784.0 | 1398.3 | 810.5 | 1014.3 |
| | M-CoMC | 0.0 | 0.0 | 0.0 | 0 | 0.0 |
| 2000–500–0.5 | Base | 28,333.6 | 4119.2 | 1321.8 | 546.6 | 587.0 |
| | M-CoMC | 5.0 | 0.0 | 1.0 | 0 | 0.0 |
| 2000–500–0.7 | Base | 13,155.0 | 3894.4 | 1464.4 | 876.8 | 428.0 |
| | M-CoMC | 0.5 | 0.0 | 0.0 | 0 | 0.0 |
| 2000–500–0.9 | Base | 2000.2 | 942.6 | 543.4 | 274.8 | 117.4 |
| | M-CoMC | 0.0 | 0.0 | 0.0 | 0 | 0.0 |
| 2000–600–0.5 | Base | 30,804.0 | 4599.0 | 1342.0 | 581.5 | 703.5 |
| | M-CoMC | 1.5 | 0.0 | 0.5 | 0 | 0.0 |
| 2000–600–0.7 | Base | 19,118.5 | 4411.3 | 1569.8 | 626.5 | 389.0 |
| | M-CoMC | 2.5 | 0.0 | 1.0 | 0 | 0.0 |
| 2000–600–0.9 | Base | 5334.6 | 2473.8 | 1194.8 | 540.8 | 95.4 |
| | M-CoMC | 0.0 | 0.0 | 0.0 | 0 | 0.0 |
| 2000–700–0.7 | Base | 21,719.4 | 4896.8 | 1601.8 | 653.6 | 478.0 |
| | M-CoMC | 0.0 | 0.0 | 0.0 | 0 | 0.0 |
| 2000–700–0.9 | Base | 7023.6 | 3325.0 | 1537.6 | 690.6 | 129.6 |
| | M-CoMC | 1.5 | 0.0 | 0.0 | 0 | 0.0 |

Note: A very small number of $TET_{low}$ and $TET_{high}$ under M-CoMC is attributed to the deceleration of mainline facilitating vehicles in the MPC process. When an HDV follows a mainline facilitating vehicle closely, a small deceleration of the facilitating vehicle may result in a TTC of less than 5 s for a very short period.

the waiting time of ramp vehicles in a merging cycle may even be longer than the average time for a ramp vehicle to merge under no controls. However, the travel delays of mainline vehicles reduce significantly by around 95%, and travel delays of all vehicles decrease by 90% on average. These can be further visualized and corroborated by the speed contours in Fig. 11. The results imply that M-CoMC sacrifices the travel time of ramp vehicles to some extent but creates much more benefits for overall systems, especially for mainline vehicles. It should be noted that the objective of M-CoMC is to minimize the delays of all vehicles in the system, as the majority of traffic control strategies do. More importantly, the situation ameliorates with higher penetration rates of CAVs. When ramp volume is 500 veh/h/lane and the penetration rate equals or over 0.5, M-CoMC can improve the travel delays of both mainline and ramp vehicles, as shown in Table 5b. When the penetration rate is 0.9, the travel delay of ramp vehicles can reduce by over 80% after M-CoMC. For the scenarios with ramp volumes of 600 and 700 veh/h/lane, the results show similar patterns as described in the scenario with a ramp volume of 500 veh/h/lane. The improvement percentages in travel delays of all vehicles after M-CoMC when ramp volumes are 600 or 700 veh/h/lane, range from 85.6% to 94.2%, which is remarked improvement in traffic efficiency.

### 5.3. Performance in merging safety

In this subsection, we demonstrate the benefits of M-CoMC in reducing collision risk in merging areas. In evaluating the safety benefit, we adopt an innovative concept of driving safety field that was proposed by Wang et al. [48]. Two safety surrogates are used to measure the rear-end collision risk at ramp merging: Time Exposed Time-to-collision (TET) and Modified Deceleration Rate to Avoid a Crash (MDRAC). These surrogates are derived from vehicle trajectory data in accordance with Minderhoud, Bovy [49] and Kuang et al. [50]. The thresholds for different risk levels are summarized in Table 6. It should be noted that we merely analyze the rear-end collision risk of HDVs, because CAVs are assumed to have advanced sensors and no reaction time, and thus deemed to avoid collisions by themselves as long as no perception and control system failure happens. Moreover, the traffic safety surrogates and thresholds are determined for measuring collision risks for human drivers with reaction times. The results averaged into one hour when the mainline volume is 2000 veh/h/lane are summarized in Table 7. Table 7 shows that there is considerable rear-end collision risk in the mainline under no controls. The $TET_{low}$ and $TET_{high}$ when ramp volume is 500 veh/h/lane and penetration rate is 0.5, are 38,231 and 5784 $s \cdot veh/h$, respectively. The $TET_{high}$ of 5,784 $s \cdot veh/h$ means that the accumulated time of vehicles under high collision risk (TTC) in one hour is 5,784 s, which hints nonnegligible risk. $MDRAC_{high}$ and $MDRAC_{critical}$ mean the period of MDRAC larger than 3.4 m/s$^2$ and TTC less than drivers' reaction time, respectively. The two surrogates are typical signals of severe collision risks. The results indicate that the accumulative time of all vehicles when the drivers have to decelerate immediately with a deceleration of larger than 3.4 m/s$^2$ to avoid potential crashes is 810.5 s. The accumulative time when TTC is less than the defined human drivers' reaction time (1 s) is 1,398.3 s. The potential reason is that the cut-in behavior of merging vehicles under no control will force the mainline vehicles to brake sharply and suddenly stop. These maneuvers will propagate upstream due to human drivers' reaction times. These can be further evidenced by the speed profiles in Fig. 11. Merging conflicts in mixed traffic with both CAVs and HDVs may be more

remarkable as compared to the scenarios with full HDVs, due to driving behavior differences between CAVs and HDVs [51]. In comparison, the traffic flow after implementing M-CoMC is free from rear-end collision risks. The reason is straightforward. The coordination between mainline facilitating vehicles and ramp platoon eliminates the merging conflicts and derivative traffic oscillation. The same results can be found when the ramp volume and penetration rate increase. These results validate the exceptional performance of the proposed control strategy in reducing rear-end collisions in the merging areas.

## 6. Conclusion

This study proposes a bi-level merging coordination strategy to facilitate ramp merging operation of mixed CAV-HDV traffic. The macro-level optimization, utilizing traffic fundamental diagrams and shock wave theories, aims to determine the optimal size of the ramp merging platoon and the cooperative merging speed. The micro-level coordination, taking the macro-level decisions and real-time traffic information as inputs, designs and updates the trajectory of controlled CAVs in each merging cycle to tackle traffic stochastics using a receding horizon scheme. The performances of the proposed control strategy are evaluated in different scenarios in terms of penetration rates (0.3, 0.5, 0.7 or 0.9), mainline volume (1,800 or 2,000 veh/h/lane), and ramp traffic volume (500, 600 or 700 veh/h/lane), based on tailored SUMO simulations for mixed traffic with heterogeneous drivers. The main findings are summarized as follows.

- M-CoMC coordinates the creation of mainline gaps and the formation of ramp platoons in mixed traffic with HDVs and CAVs. The coordination is achieved as expected under high traffic volumes and various CAV penetration rates.
- M-CoMC smoothens vehicle merging trajectories and eliminates traffic oscillations on the mainline freeway.
- M-CoMC can notably reduce the travel delays of all vehicles in the merging areas under different scenarios in terms of mainline volume, ramp volume and penetration rates of CAVs. M-CoMC can reduce the travel delays of all vehicles by around 90% on average when mainline volumes are 1800 and 2000 veh/h/lane.
- In most cases, M-CoMC benefits both the mainline and ramp traffic. However, in a few cases (large mainline/ramp volume and low penetration rate of CAVs), the travel delays of ramp vehicles under M-CoMC are larger than those without control. The efficiency benefits of M-CoMC are more notable under high to congested traffic volumes. This indicates a need to introduce an activation threshold of M-CoMC in terms of traffic volume and CAV penetration rate in practice.
- M-CoMC can eliminate the collision risk in merging areas via efficient coordination.

This study has some limitations that need to be improved through future research. First, this study uses assumptions and hypothetical parameters for the CAV following/lane-changing model due to limited access to field test data of fully automated CAVs. This needs to be improved in the future when more CAV empirical studies become available. However, it is worth noting that the current models considering stochastic traffic patterns and heterogenous driving behaviors are more realistic than most simulation practices in the existing literature. Further, we assume and implement a prohibition of lane changing to the outside lane before the merging area if there are multiple lanes in the mainline. However, the HDVs may not follow the rule and cut into the gap in front of the mainline facilitating vehicle [54]. The receding horizon control at the micro level can address this issue to some extent but not comprehensively. It is worth exploring more robust and rigorous control methods at both macro and micro levels considering the potential illegal cut-in behavior before the merging area in future work. Meanwhile, this study ignores free lane changing between mainline lanes. One possible way is to use the theory of “moving bottlenecks” to depict the influences of lane-changing behavior before the merging area [55,56] and extend the optimization at the macro level to consider the influences of lane changing behavior. When multiple lanes exist on the mainline freeway, there is a potential to include courtesy lane changing (i.e., proactive lane changing from outer lane to inner lanes) in the coordination to facilitate ramp merging further. Meanwhile, the trajectory planning method in Section 3.2.3 can be further improved to consider other objectives (such as energy consumption) by more advanced trajectory planning approaches. The focus of ongoing research is to address the limitations above and extend the application context of the proposed coordination strategy. Last but not least, the proposed coordination strategy focuses on dense traffic (but not congested) situations. If the traffic in the mainline and ramp are already congested or broken down, other tailored control for congested situations should be implemented instead, which is one of the interesting directions to explore in future work.

## Declaration of competing interest

The authors declare that they have no conflicts of interest in this work.

## CRediT authorship contribution statement

**Jie Zhu:** Conceptualization, Methodology, Formal analysis, Writing – original draft. **Kun Gao:** Conceptualization, Methodology, Formal analysis, Writing – original draft. **Hao Li:** Validation, Supervision, Writing – review & editing. **Zijing He:** Validation, Writing – review & editing. **Cristina Olaverri Monreal:** Conceptualization, Validation, Supervision, Writing – review & editing.

## Acknowledgement

The authors are grateful to VINNOVA (ICV-safety), National Key R&D Program of China, 2019YFE0108300, and the Area of Advance Transport and AI Center (CHAIR) at Chalmers University of Technology for funding this research.

## Appendix

We also compare the proposed coordination with the typical local feedback ramp control strategy ALINEA in the scenarios with mainline traffic volume 2000 veh/h/lane and ramp traffic volume (500 and 600 veh/h/lane). Referring to the literature [1,2], the implemented ALINEA strategy at each period $k = 1,2,\ldots$ (every minute) is formulated as

$$r(k) = r(k-1) + K_R(\hat{O} - O_{out}(k)) \tag{A.1}$$

$$g = \left(\frac{r(k)}{r_{sat}}\right)C \tag{A.2}$$

where $r(k)$ is on-ramp traffic volume that may be controlled using traffic lights at the $k^{\text{th}}$. $r(k-1)$ is set equal to the measured actual ramp volume in the last period. $O_{out}(k)$ is the occupancy at the downstream of the merging point and is measured by an inductive loop detector shown in Fig. A.1. $K_R$ is the regulator parameter and set to be 70 vph referring to Papageorgiou et al. (1997). $\hat{O}$ is set to be 28 (%) based on the occupancy at capacity derived from Eqs. (45)-(47) in the revised manuscript. g is the green time and is constrained in the range $[0.1C, C]$. C is the fixed traffic cycle duration and set to be 90 s referring to Papageorgiou et al. (1997). $r_{sat}$ is ramp capacity flow and set to be 1,800 vph.

We compare the results between the proposed strategy and ALINEA using SUMO based on the same traffic flow and road network. The results are summarized in Table A.1 and show that the proposed coordination has better performance for reducing delays as compared to ALINEA.

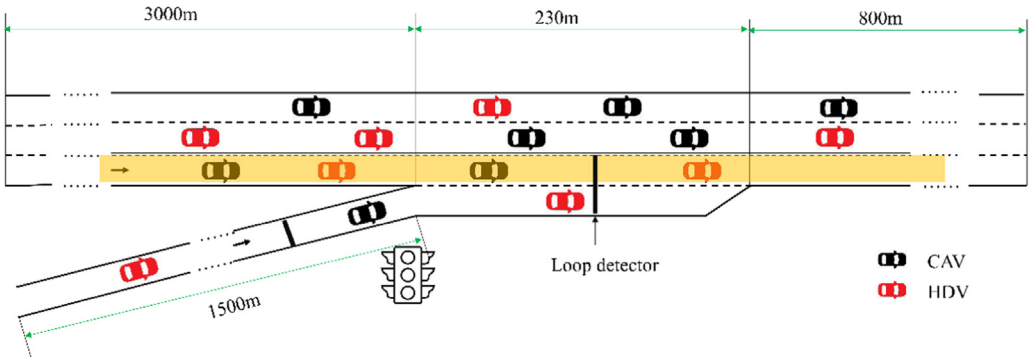


**Fig. A.1. ALINEA demonstration.**

**Table A.1**
**The comparison between the proposed coordination and ALINEA.**

| Scenarios (Mainline volume - ramp volume - penetration) | | Average delay (seconds) | | | Delay reduction | | |
|---|---|---|---|---|---|---|---|
| | | Overall | Main | Ramp | Overall | Main | Ramp |
| 2000–500–0.5 | ALINEA | 111.56 | 106.4 | 131.33 | −82.8% | −90.2% | −59.5% |
| | M-CoMC | 19.2 | 10.4 | 53.2 | | | |
| 2000–500–0.7 | ALINEA | 91.41 | 62.25 | 210.51 | −83.5% | −87.9% | −79.7% |
| | M-CoMC | 13.8 | 6.3 | 42.8 | | | |
| 2000–600–0.5 | ALINEA | 127.36 | 108.43 | 221.79 | −69.0% | −79.1% | −59.1% |
| | M-CoMC | 31.4 | 14.3 | 90.7 | | | |
| 2000–600–0.7 | ALINEA | 69.45 | 43.89 | 162.92 | −76.4% | −80.9% | −73.3% |
| | M-CoMC | 16.4 | 8.4 | 43.5 | | | |
| 2000–600–0.9 | ALINEA | 58.16 | 43.46 | 120.50 | −75.9% | −79.1% | −71.5% |
| | M-CoMC | 11.6 | 4.9 | 34.3 | | | |
| Average all scenarios | | | | −77.5% | −83.4% | −68.6% | |

## References

[1] M. Papageorgiou, H. Hadj-Salem, J.-M. Blosseville, ALINEA: a local feedback control law for on-ramp metering, Transp. Res. Rec. 1320 (1) (1991) 58–67.
[2] M. Papageorgiou, H. Hadj-Salem, F. Middelham, ALINEA local ramp metering: summary of field results, Transp. Res. Rec. 1603 (1) (1997) 90–98.
[3] R.C. Carlson, I. Papamichail, M. Papageorgiou, Local feedback-based mainstream traffic flow control on motorways using variable speed limits, IEEE Trans. Intell. Transp. Syst. 12 (4) (2011) 1261–1276.
[4] A. Hegyi, B. De Schutter, H. Hellendoorn, Model predictive control for optimal coordination of ramp metering and variable speed limits, Transp. Res. Part C: Emerg. Technol. 13 (3) (2005) 185–209.
[5] J. Zhang, T.-Q. Tang, Y Yan, Eco-driving control for connected and automated electric vehicles at signalized intersections with wireless charging, Appl. Energy 282 (2021) 116215.
[6] X. Qu, Z. Zeng, K Wang, Replacing urban trucks via ground–air cooperation, Commun. Transp. Res. 2 (2022) 100080.
[7] Y. Wang, W. E, W.et al. Tang, Automated on-ramp merging control algorithm based on Internet-connected vehicles, IET Intel. Transport Syst. 7 (4) (2013) 371–379.
[8] J. Zhu, S. Easa, K. Gao, Merging control strategies of connected and autonomous vehicles at freeway on-ramps: a comprehensive review, J. Intell. Connected Veh. (2022) (EarlyCite), doi:10.1108/JICV-02-2022-0005.
[9] W. Cao, M. Mukai, T Kawabe, Cooperative vehicle path generation during merging using model predictive control with real-time optimization, Control Eng. Pract. 34 (2015) 98–105.
[10] Y. Zhou, M.E. Cholette, A. Bhaskar, et al., Optimal vehicle trajectory planning with control constraints and recursive implementation for automated on-ramp merging, IEEE Trans. Intell. Transp. Syst. 20 (9) (2019) 3409–3420, doi:10.1109/TITS.2018.2874234.
[11] S. Fukuyama, Dynamic game-based approach for optimizing merging vehicle trajectories using time-expanded decision diagram, Transp. Res. Part C: Emerg. Technol. 120 (2020) 102766.
[12] A. Dabiri, B. Kulcsár, Incident indicators for freeway traffic flow models, Comm. Transp. Res. 2 (2022) 100060.
[13] I.A. Ntousakis, I.K. Nikolos, M. Papageorgiou, Optimal vehicle trajectory planning in the context of cooperative merging on highways, Transp. Res. Part C: Emerg. Technol. 71 (2016) 464–488.
[14] C. Letter, L. Elefteriadou, Efficient control of fully automated connected vehicles at freeway merge segments, Transp. Res. Part C: Emerg. Technol. 80 (2017) 190–205.
[15] Y. Xie, H. Zhang, N.H. Gartner, Collaborative merging strategy for freeway ramp operations in a connected and autonomous vehicles environment, J. Intell. Transp. Syst. 21 (2) (2017) 136–147.
[16] J. Rios-Torres, A.A. Malikopoulos, Automated and cooperative vehicle merging at highway on-ramps, IEEE Trans. Intell. Transp. Syst. 18 (4) (2017) 780–789.
[17] S. Acharya, M. Mekker, Importance of the reputation of data manager in the acceptance of connected vehicles, Comm. Transp. Res. 2 (2022) 100053.
[18] L. Xu, J. Lu, B Ran, Cooperative merging strategy for connected vehicles at highway on-ramps, J. Transp. Eng., Part A: Systems 145 (6) (2019) 04019022.
[19] J. Ding, L. Li, H Peng, A rule-based cooperative merging strategy for connected and automated vehicles, IEEE Trans. Intell. Transp. Syst. 21 (8) (2020) 3436–3446.
[20] S. Jing, F. Hui, X Zhao, Cooperative game approach to optimal merging sequence and on-Ramp merging control of connected and automated vehicles, IEEE Trans. Intell. Transp. Syst. 20 (11) (2019) 4234–4244.
[21] N. Chen, B. van Arem, T Alkim, A hierarchical model-based optimization control approach for cooperative merging by connected automated vehicles, IEEE Trans. Intell. Transp. Syst. (2020) (Early Access), doi:10.1109/TITS.2020.3007647.
[22] M. Karimi, C. Roncoli, C Alecsandru, Cooperative merging control via trajectory optimization in mixed vehicular traffic, Transp. Res. Part C: Emerg. Technol. 116 (2020) 102663.
[23] Z. Sun, T. Huang, P. Zhang, Cooperative decision-making for mixed traffic: a ramp merging example, Transp. Res. Part C: Emerg. Technol. 120 (2020) 102764.
[24] H. Okuda, T. Suzuki, K Harada, Quantitative driver acceptance modeling for merging car at highway junction and its application to the design of merging behavior control, IEEE Trans. Intell. Transp. Syst. 22 (1) (2021) 329–340.
[25] Z.E.A. Kherroubi, S. Aknine, R. Bacha, Novel decision-making strategy for connected and autonomous vehicles in highway on-ramp merging, IEEE Trans. Intell. Transp. Syst. (2021) (Early Access), doi:10.1109/TITS.2021.3114983.
[26] A. Omidvar, L. Elefteriadou, M Pourmehrab, Optimizing freeway merge operations under conventional and automated vehicle traffic, J. Transp. Eng., Part A: Systems 146 (7) (2020) 04020059.
[27] X. Qu, L. Zhong, Z Zeng, Automation and connectivity of electric vehicles: energy boon or bane? Cell Rep. Phys. Sci. 3 (8) (2022) 101002.
[28] Zhu, J., Tasic, I., Qu, X.: Improving freeway merging efficiency via flow-level coordination of connected and autonomous vehicles. (2021).
[29] J. Zhu, I. Tasic, X. Qu, Flow-level coordination of connected and autonomous vehicles in multilane freeway ramp merging areas, Multimodal Transp. 1 (1) (2022) 100005.
[30] E. Ward, N. Evestedt, D Axehill, Probabilistic model for interaction aware planning in merge scenarios, IEEE Trans. Intell. Veh. 2 (2) (2017) 133–146.
[31] DLR: interfacing TraCI from Python. https://sumo.dlr.de/docs/TraCI/Interfacing_TraCI_from_Python.html (2021).
[32] M.-R. Sonbolestan, S. Monajjem, E. Rouhani, Impact of optimal selection of merging position on fuel consumption at highway on-ramps, J. Transp. Eng., Part A: Systems 147 (5) (2021) 04021023.
[33] M.N. Sharath, N.R. Velaga, Enhanced intelligent driver model for two-dimensional motion planning in mixed traffic, Transp. Res. Part C: Emerg. Technol. 120 (2020) 102780.

[34] A. Sharma, Z. Zheng, A. Bhaskar, et al., Modelling car-following behaviour of connected vehicles with a focus on driver compliance, Transp. Res. Part B: Methodological 126 (2019) 256–279.
[35] A. Alhariqi, Z. Gu, M. Saberi, Calibration of the intelligent driver model (IDM) with adaptive parameters for mixed autonomy traffic using experimental trajectory data, Transportmetrica B: Transp. Dyn. 10 (1) (2022) 421–440.
[36] H. Yu, R. Jiang, Z He, Automated vehicle-involved traffic flow studies: a survey of assumptions, models, speculations, and perspectives, Transp. Res. Part C: Emerg. Technol. 127 (2021) 103101.
[37] M. Zhu, X. Wang, A. Tarko, Modeling car-following behavior on urban expressways in Shanghai: a naturalistic driving study, Transp. Res. Part C: Emerg. Technol. 93 (2018) 425–445.
[38] C.P.I.J. van Hinsbergen, W.J. Schakel, V.L. Knoop, A general framework for calibrating and comparing car-following models, Transportmetrica A: Transp. Sci. 11 (5) (2015) 420–440.
[39] M. Zhou, X. Qu, S. Jin, On the impact of cooperative autonomous vehicles in improving freeway merging: a modified intelligent driver bodel-based approach, IEEE Trans. Intell. Transp. Syst. (2017) 1–7.
[40] U. Durrani, C. Lee, D. Shah, Predicting driver reaction time and deceleration: comparison of perception-reaction thresholds and evidence accumulation framework, Accident Anal. Prevent. 149 (2021) 105889.
[41] J. Erdmann, SUMO's lane-changing model, in: Modeling Mobility with Open Data, Springer, 2015, pp. 105–123.
[42] W. Daamen, M. Loot, S.P. Hoogendoorn, Empirical analysis of merging behavior at freeway on-ramp, Transp. Res. Rec. 2188 (1) (2010) 108–118.
[43] J.-T. Kim, J. Kim, M. Chang, Lane-changing gap acceptance model for freeway merging in simulation, Can. J. Civ. Eng. 35 (3) (2008) 301–311.
[44] Y. Li, L. Zhao, K. Gao, et al., Revealing driver psychophysiological response to emergency braking in distracted driving based on field experiments, J. Intell. Connect. Veh. 5 (3) (2022) 270–282.
[45] L. Yue, M. Abdel-Aty, Z. Wang, Effects of connected and autonomous vehicle merging behavior on mainline human-driven vehicle, J. Intell. Connect. Veh. 5 (1) (2022) 36–45.
[46] DLR: Definition of vehicles, vehicle types, and routes. https://sumo.dlr.de/docs/Definition_of_Vehicles%2C_Vehicle_Types%2C_and_Routes.html#lane-changing_models (2021).
[47] TRB, Highway capacity manual - a guide for multimodal mobility analysis (6th Edition), Transp. Res. Board (2016).
[48] J. Wang, J. Wu, Y. Li, The driving safety field based on driver–vehicle–road interactions, IEEE Trans. Intell. Transp. Syst. 16 (4) (2015) 2203–2214.
[49] M.M. Minderhoud, P.H.L. Bovy, Extended time-to-collision measures for road traffic safety assessment, Accident Anal. Prevent. 33 (1) (2001) 89–97.
[50] Y. Kuang, X. Qu, J. Weng, How does the driver's perception reaction time affect the performances of crash surrogate measures? PLoS One 10 (9) (2015).
[51] Z. Yao, R. Hu, Y. Jiang, Stability and safety evaluation of mixed traffic flow with connected automated vehicles on expressways, J. Safety Res. 75 (2020) 262–274.
[52] K. Gao, H. Tu, L. Sun, et al., Impacts of reduced visibility under hazy weather condition on collision risk and car-following behavior: implications for traffic control and management, Int. J. Sustain. Transp. 14 (8) (2020) 635–642.
[53] A. Arun, M.M. Haque, A. Bhaskar, et al., A systematic mapping review of surrogate safety assessment using traffic conflict techniques, Accident Anal. Prevent. 153 (2021) 106016.
[54] Q. Xue, K. Gao, Y. Xing, et al., A context-aware framework for risky driving behavior evaluation based on trajectory data, IEEE Intell. Transp. Syst. Mag. 12 (2021) 1–12.
[55] O. Hui, T. Tie-Qiao, Impacts of moving bottlenecks on traffic flow, Physica A 500 (2018) 131–138.
[56] C.F. Daganzo, J.A. Laval, On the numerical treatment of moving bottlenecks, Transp. Res. Part B: Methodological 39 (1) (2005) 31–46.

**Jie Zhu** recently received the Ph.D. degree in transportation engineering from the Chalmers University of Technology, Gothenburg, Sweden. She holds a B.Sc. degree in transportation engineering from Tongji University, Shanghai, China, and a M.Sc. degree in civil engineering from Technical University of Munich, Germany. She is currently a research engineer with Volvo Technology AB. Her research focuses on connected and autonomous vehicles, including V2X communication, autonomous perception and control, maneuver coordination and trajectory planning, and traffic flow level operation.

**Kun Gao** is currently an assistant professor in the Department of Architecture and Civil Engineering, Chalmers University of Technology (CTH). He received his Bachelor and Ph.D. degrees from Tongji University. His works on promoting sustainable mobility focusing on electrification, shared mobility, and connected automation, especially establishing new approaches and tools for system planning, optimization and evaluation of emerging transport systems leveraging big data and machine learning. He has successfully secured research projects (over 16 million SEK in total) as a principal investigator. He published over 30 articles in journals of transportation engineering and interdisciplinary areas including *Transportation*, *Transportation Research Part A*, *Part D*, and *Part F*.

**Hao Li** is a professor in the College of Transportation Engineering, Tongji University. She received the B.Sc. degree in civil engineering from Tongji University, Shanghai, China, and the M.Sc. and Ph.D. degrees in transportation and planning from Delft University of Technology, Delft, the Netherlands. Her main research interests include transport network modeling, network design, travel behavior under uncertainty, and network reliability. She received the Best Scientific Paper Award at the 14th World Congress on Intelligent Transport Systems, Beijing, China. She also received the National Natural Science Foundation of China (NSFC) Grant and is currently managing two projects funded by the Ministry of Education.

**Cristina Olaverri-Monreal** is holding the BMK endowed professorship and chair for sustainable transport logistics 4.0 at Johannes Kepler University, Linz, 4040, Austria. Her research interests include automated driving, advanced driving assistance systems, human-factors and human–machine interaction, sustainable transport, and simulation tools.